Tânia Isabel Rodrigues Genebra

Immobilization of Metalloproteins for Biotechnological Applications

Dissertação de Mestrado em Ciências Farmacêuticas, especialidade Biotecnologia Farmacêutica, orientada pela Doutora Smilja Todorovic (ITQB-UNL) e pelo Professor Doutor Luís Almeida e apresentada na Faculdade de Farmácia da Universidade de Coimbra.

Setembro 2012

· U C ·

UNIVERSIDADE DE COIMBRA

Dissertation submitted to the Faculty of Pharmacy, University of Coimbra in order to obtain the master degree in Pharmaceutical Biotechnology.

Coimbra 2012

Work performed under the scientific orientation of:

Dr. Smilja Todorovic

Laboratory of Raman Spectroscopy of Metalloproteins at ITQB-UNL.

and

Professor Dr. Luís Almeida

Faculty of Pharmacy at University of Coimbra

AKNOWLEDGEMENTS

I acknowledge Dr. Smilja Todorovic, for giving me a great opportunity, especially for the trust and shared knowledge. I appreciate the opportunity to have had this work done in the Laboratory for Raman Spectroscopy of Metalloproteins (RSM) at Instituto de Tecnologia Química e Biológica da Universidade Nova de Lisboa (ITQB-UNL) under her orientation.

The ITQB-UNL for the opportunity to conduct this research.

Three magnificent coordinators of master of Pharmaceutical Biotechnology, Faculty of Pharmacy of University of Coimbra, Prof. Dr. João Nuno, Prof. Dr. Luis Almeida and Prof. Dr. Sérgio Simões, without their help and dedication it would be impossible to achieve this step.

Dr. Lígia O. Martins and Sonia Mendes for the knowledge shared during the purification of the enzyme in the "Enzyme & Microbial Technology" Laboratory at ITQB-UNL.

Dr. Murat Sezer, for friendship and companionship during months of practical realization of this dissertation.

My parents, José and Jacinta, and my sister, Dora, who accompanied me in this trajectory. Thank you for believing in me.

To a very special friend who was always available during this time, for his friendship and understanding in difficult times of this work.

To all my friends and colleagues at ITQB and Faculty of Pharmacy, where I often found understanding, encouragement and support.

ABSTRACT

Heme peroxidases couple the oxidation of a variety of organic substrates with reduction of H_2O_2 to water. They represent an attractive platform for both detection and monitoring of H_2O_2 and biocatalysis of organic compounds. DyP-type peroxidases constitute a novel family of heme peroxidases. They are capable of efficient decolourisation of several dyes, including anthraquinone-based and azo dyes that are of industrial and environmental relevance. DyPs are unrelated to other known peroxidases with respect to primary sequence, catalytic properties and tertiary structure. In this work we establish the first step towards exploring the potential of DyP-type peroxidases for biotechnological applications. We present a purification and combined biochemical, spectroscopic and spectro-electrochemical study of a recombinant DyP-type peroxidase from *Pseudomonas putida* MET94 (PpDyP) immobilized on bio-compatibly coated Ag electrodes. The aim of this work is to provide structural and mechanistic insights into an immobilized DyP-type peroxidase, as a basis for a rational design of bio-electronic device(s) employing PpDyP.

Keywords: DyP-type peroxidase, biosensors, resonance Raman spectroscopy, biotechnological application, heme proteins, SERR.

RESUMO

Peroxidases hémicas oxidam uma vasta variedade de substratos orgânicos mediante a redução de H_2O_2 a água. Estas enzimas representam uma plataforma atraente para a detecção e monitorização de H_2O_2 bem como para a biocatálise de compostos orgânicos. DyP peroxidases constituem uma nova família de peroxidases hémicas, capazes de descolorarem eficientemente vários corantes, incluindo corantes derivados da antraquinona quer corantes azo e que são de elevado interesse industrial e ambiental. Estas peroxidases não estão relacionadas com outras peroxidases já conhecidas, quer no que diz respeito à sua sequência primária, quer propriedades catalíticas e até estrutura terciária. Neste trabalho, pretende-se estabelecer o primeiro passo para explorar o potencial de DyPs para aplicações biotecnológicas. É apresentada a purificação combinada com um estudo SERR espectro-eletroquímico de uma DyP recombinante, obtida a partir de *Pseudomonas putida* MET94 (PpDyP), imobilizada num eléctrodo biocompatìvel de prata (Ag). O objectivo deste trabalho é fornecer informações estruturais e mecanicistas sobre uma DyP imobilizada, como base para um desenho racional de um dispositivo bioelectrónico (biosensor) baseado nessa mesma proteína (PpDyP).

Palavras-chave: DyP, biosensores, espectroscopia de resonância de Raman, aplicações biotecnológicas, proteínas hémicas, SERR.

CONTENTS

1.1. Objective

The objective of this work is the characterization of a novel enzyme, Dye decolorizing peroxidase (DyP) from *Pseudomonas putida* (PpDyP). We aim to learn about biochemical, structural and catalytic properties of the enzyme in solution, in order to contribute to better understanding of DyPs, a novel family of heme peroxidases, in general. Moreover, we aim to address the properties of immobilized PpDyP, in order to explore its potential for biotechnological applications. Being a heme peroxidase, DyP catalyses the reduction of hydrogen peroxide to water, utilizing a variety of electron donors. In this manner, DyPs represent a promising platform for design of enzyme electrodes that can be used in construction of biosensor and/or biocatalysts for detection or processing of either of the substrates (Fig. 1) [1]. An important strategy in the design of such biosensors and biocatalysts is the immobilization of enzymes onto conductive support materials. The performance of the biodevice is then determined by the structural integrity, functionality and stability of the immobilized enzyme and efficiency of electronic communication, between the enzyme and the conductive support material [2]. One of the most prominent examples of biosensors is the Glucose oxidase based glucose detecting device. This enzyme has been widely used as a sensor for biorecognition of glucose, due to the need for determination / monitoring of glucose in patients with diabetes.

This work is divided in two stages: i) the purification and the biochemical characterization of enzyme and ii) structural characterization of the protein in solution and in immobilized state. First, it was necessary to purify a sufficient amount of the enzyme. We optimized the procedure for transformation of the expression vector containing the recombinant gene into an *Escherichia coli* strain (heterologous expression). Then we purified protein and characterized its biochemical and catalytic properties and stability.

In the next step we employed vibartional spectroscopy that helped us to characterize physiologically relevant configurational state(s) of PpDyP heme group. We took advantage of high selectivity and sensitivity of surface enhanced Resonance Raman (SERR) spectroscopy and spectroelectrochemistry to describe structural and thermodynamic properties of the enzyme immobilized onto biocompatible metal electrodes.

The outcome of this work is expected to have an impact on development of alternative ways for: i) dye processing and treatment of toxic industrial chemicals and wastes, including pollutants such as phenols and pesticides, which are not amenable to biological wastewater treatments, and ii) H_2O_2 detection, relevant in environmental, pharmaceutical, clinical and industrial analysis. Moreover, this work could shed some light onto physiological features of a new member of a novel heme peroxidise family which was not investigated before.

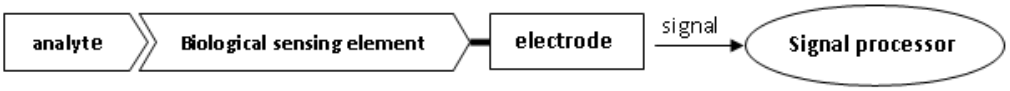

Figure 1 – *Schematic representation of the design of an electrochemical biosensor.*

2.1. Peroxidase superfamily

Heme peroxidases oxidize organic substrates using hydrogen peroxide as electron acceptor. Degradation of hydrogen peroxide into O_2 and H_2O arises in cells as a result of oxygen metabolism, imposing a special role in cellular detoxification mechanism to peroxidases [3]. Nowadays peroxidases can be used for various applications, mainly for decontamination of soil and water. There are numerous ongoing investigations on application of peroxidases in industrial processes, such as food control, as well as medicine-related areas [4]. For instance, in immunohistochemistry, horseradish peroxidase (HRP) is used to detect antibodies that may be an evidence of metabolic disfnctions such as thyroid disease. It is also used as a diagnostic tool in pathology as it has the ability to target and bind to certain biomarkers found in cancers [5]. Therefore, a better understanding of HRP and peroxidases in general could lead to a new targeted cancer therapy [6].

2.1.1. Classification of peroxidases

Peroxidases can be classified as non-heme and heme (Fig.2). Heme peroxidases catalyze the peroxidation of substrates employing an iron ion present in heme active center. In the resting state, the heme group of the heme peroxidases is in ferric oxidation state (Fe III). The members of non-heme peroxidases in the active site have one redox cysteine or selenocysteine [7].

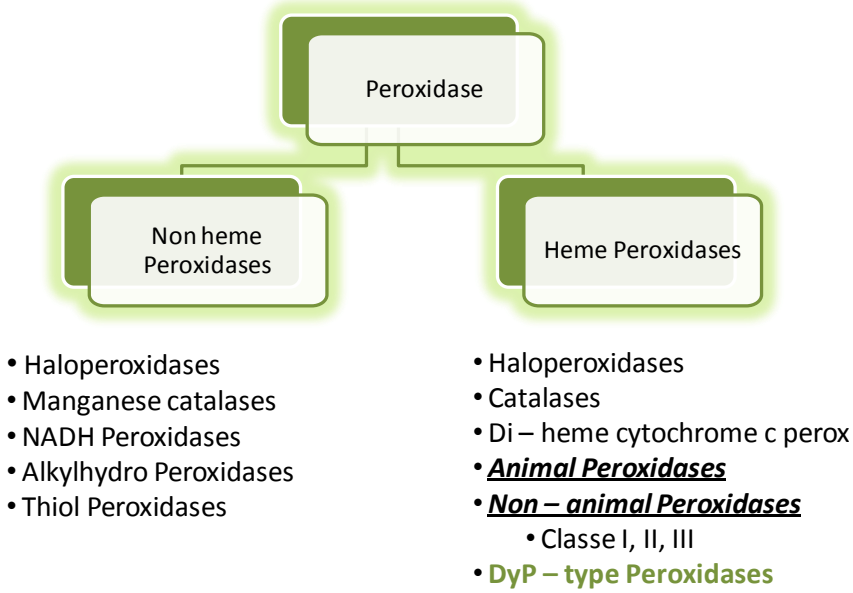

Figure 2 – *Classification of peroxidases*

Heme peroxidase family was originally divided into two super families: the animal peroxidases and the plant peroxidases. The latter is divided into three classes, class I, II and III [7] but nowadays there are more families such as Catalases, Haloperoxidases for instance (Fig. 2).

- ***Class I*** (Procaryotic) – These enzymes are involved in plant detoxification (elimination of hydrogen peroxide). These include the yeast cytochrome c peroxidase (CcP), ascorbate peroxidases (APX) and bacterial catalase-peroxidases (BCPX). These peroxidases do not have disulfide bonds, Ca^{2+} ions or signal peptides for secretion and they are not glycosylated. The triptofan (Trp117 in CcP) is conserved in all members of the class I [7].

- ***Class II*** (Fungal) – These enzymes include lignin and manganese peroxidase (LiP and MnP respectively), involved in lignin degradation. They have 5% of carbohydrates, four highly conserved disulfide bridges and two structurally important Ca^{2+} ions. The conserved Trp (Trp117 in CcP) residue present in the class I is replaced by phenylalanine (Phe190 in MnP) or leucine [7].

- ***Class III*** (Plant) – In addition the most widely studied HRP, this group also includes barley (BP), peanut (PNP) and soybean (SBP) peroxidases. Structurally, these enzymes have a signal peptide at the N-terminal, two Ca^{2+} ions and four conserved disulfide bridges at different places than class II enzymes, a set of helices that plays an important role in the binding of substrate, and some degree of glycosylation [7].

Recently, novel peroxidases have been described. These peroxidases are capable of decolorizing dyes. They lack homology in their primary and tertiary structure with the known peroxidases, leading to establishment of a new family, called DyP-type Peroxidases.

- **DyP type Peroxidases** (dye-decolourising type peroxidases) - These enzymes exhibit only low homology sequence to fungal peroxidases, such as LiP and MnP, and do not contain the conserved distal His (His46 in MnP) and the essential Arg (Arg 42 in MnP) found in all other plant peroxidases [7].

2.1.2. Structural properties of Heme Peroxidases

The best known and most widely studied peroxidase is the HRP. HRP is a metalloenzyme that exists in the root of the horseradish plant. It uses hydrogen peroxide to oxidize both organic and inorganic compounds [8]. This enzyme along with other heme peroxidases is brightly colored due to the presence of heme cofactor.

- **Active center**

The active center of resting heme peroxidases has a *heme b* cofactor (i.e. ferriprotoporphyrin IX) (Fig. 3), constituted by four pyrrole rings and a metal ion in ferric oxidation state, Fe^{3+} [9]. In peroxidases, the iron ion is typically pentacoordinated, with the fifth proximal coordination position occupied by a His (His170 in HRP).

The sixth axial position of iron is vacant in the resting state [8]. This site is open for hydrogen peroxide to bind during the catalytic reaction. The binding of heme group to the protein does not occur only through the proximal coordination but also through other interactions such as hydrogen bonding between side chains and propionate substituents and hydrophobic interactions between hydrophobic amino acids and the porphyrin ring [9].

The catalytic reaction occurs at the distal side of the heme and during the reaction the iron adopts different spin and oxidation states (see below).

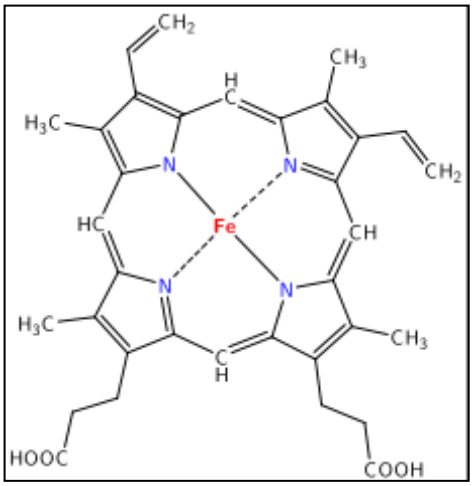

Figure 3 – *Structure of heme b group.*

Figure 4 shows the three-dimensional structure of HRP. In this enzyme both, heme group and calcium atoms are crucial for the proper working of the enzyme. The loss of one calcium atom results in instability of HRP [6]. According to Veitch, "Each calcium site is seven-coordinate with oxygen-donor ligands provided by a combination of amino acid side-chain carboxylates (Asp), hydroxyl groups (Ser, Thr), backbone carbonyls and a structural water molecule (distal site only)" [6].

Figure 4 – *Three dimensional structure of horseradish peroxidase, where the heme group is located in the middle with the iron atom represented in red. The calcium ions are shown in black and the α-helical and β-sheets are surrounding the heme [10].*

- **Catalytic reaction**

Peroxidases catalyze the oxidation of several substrates, mainly phenolic compounds , using H_2O_2 as electron acceptor (Fig.5). Typically H_2O_2 oxidizes the native enzyme [Fe^{3+}] by a two electron steps to generate a radical cation (oxoferryl heme), called Compound I (Co I): one electron is removed from iron and another electron is removed from porphyrin. The Co I accepts an electron and a proton from a substrate (RH) to generate the corresponding free radical (R●) and an oxo-ferryl intermediate called Compound II (Co II). In the next step of monoelectronic reduction of Co II, a second molecule of RH regenerates the enzyme into its resting ferric form [11,12]. Compound III (Co III) (Fe^{3+}- $O_2H^{\cdot}$) has been identified as a product formed in the presence of excess of H_2O_2 [13].

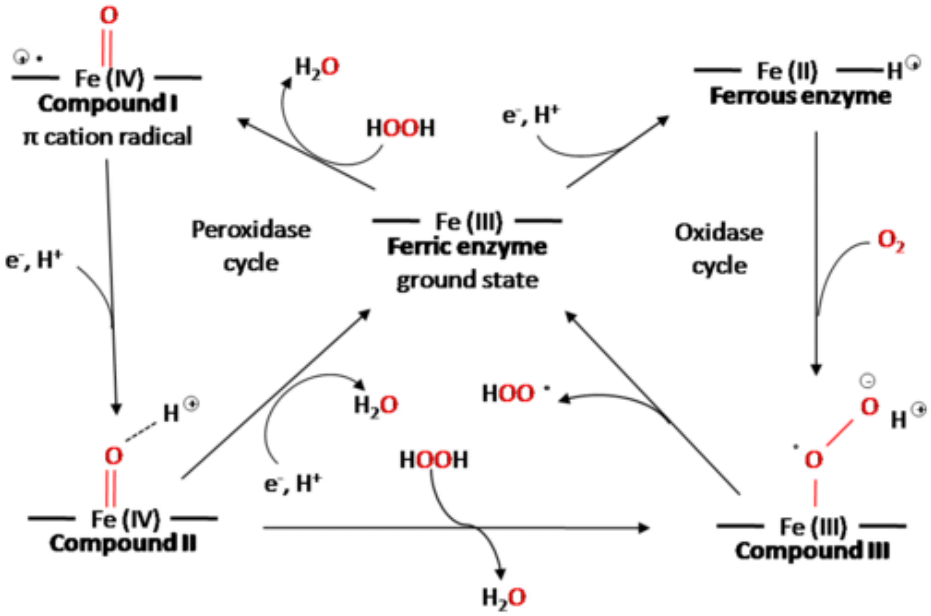

Figure 5 – *Generic catalytic cycle of a peroxidase [10].*

The reaction mechanism is conserved in all class III peroxidases.

In the distal area the most important residues are arginine (Arg 38 in HRP), histidine (His 4 in HRP) and asparagine (Asn 70 in HRP), this latter binds to histidine (His 4 in HRP) via hydrogen bonding [6]. In HRP the proximal histidine (His 170) occupying the fifth coordination position of heme iron is hydrogen bonded to the aspartic acid (Asp 247) located in the proximal area. This link is fully preserved in peroxidases. Axial ligands contribute to the low reduction potential of the heme iron. In formation of Co I the temporal electron donor may be an aminoacid instead of the porphyrin ring, generating a free radical based on a residue. Apparently, the localization of the free radical also influences the redox potential of peroxidases [11].

The distal cavity in peroxidases is the site of interaction with H_2O_2. It is characterized by two completely invariant residues in class III peroxidases, which are the distal histidine and arginine, that generate a hydrophilic hollow. When iron is pentacoordinated the fifth ligand pushes it out of the heme plane. In some peroxidases the iron is coordinated by water as the sixth axial ligand, but it is not always the case since a network of water molecules, which forms a multiple hydrogen bonds, preventing the coordination of water as sixth ligand. Distal histidne and arginine have a large involvement in the formation and stabilization of Co I [14]. H_2O_2 transfers a proton to the distal histidine, deprotonated when the enzyme is active.

This conformation is stable for the formation of hydrogen bond between distal histidine and oxygen of the side chain of asparagine. The nitrogen atom of the histidine side chain acts as an acceptor of protons, keeping hydrogen peroxide at the position of the sixth ligand of heme iron. The distal histidine therefore serves as a catalyst of the acid-base reaction with hydrogen peroxide and the side chain of arginine residue stabilizes the charge during the formation of the Co I [8]. The reaction cycle is irreversible, since the reaction rate of formation is higher than the rate of dissociation [12]. Formed catalytic intermediates have a very short half life and are very difficult to detect [11]. Nevertheless, they possess distinct UV-Vis and RR spectroscopic fingerprints.

2.1.3. Redox potential

Redox potential (E°) is a catalytically relevant thermodynamic property of heme enzymes [11]. Peroxidases display a more negative Fe(III)/Fe(II) redox potential than other heme proteins. Therefore, ferric state of the heme is stabilized in peroxidases, suggesting that inside the protein matrix, higher iron oxidation states such as Fe (IV) or Fe (V) would also be sufficiently stabilized to be transiently present during the catalytic reaction. Additionally, aqueous Fe (III) is able to react with H_2O_2 in order to generate hydroxyl radicals (Fenton reaction) [11].

For peroxidases, the relevant catalytic intermediates are Co I and Co II. However, Fe(III)/Fe(II) redox potential could still be a useful indicator of the oxidizing character of peroxidases. More positive Fe(III)/Fe(II) redox potential indicates a higher electron deficiency within the active site, and the existence of enzymatic intermediates with higher oxidative capacity. The redox potentials Fe (III)/Co I, Co I/Co II and Co II/Fe (III) can be estimated by different methods based on spectral determination of equilibrium between redox species, or use of catalytic measurements [8]. For example, in HRP E° (Fe (III)/Fe (II)) is -278 mV (vs Ag/AgCl), E° (Co I/Co II) is 880 mV (vs Ag/AgCl) and E° (Co II/Fe(III)) is 890 mV (vs Ag/AgCl)[11].

2.1.4. Biotechnological applications

Peroxidases can be employed as i) biocatalysts for formation/degradation of a large number of diverse compounds and ii) as biosensors for detection of hydrogen peroxide or other substrates in the environment (Fig. 6).

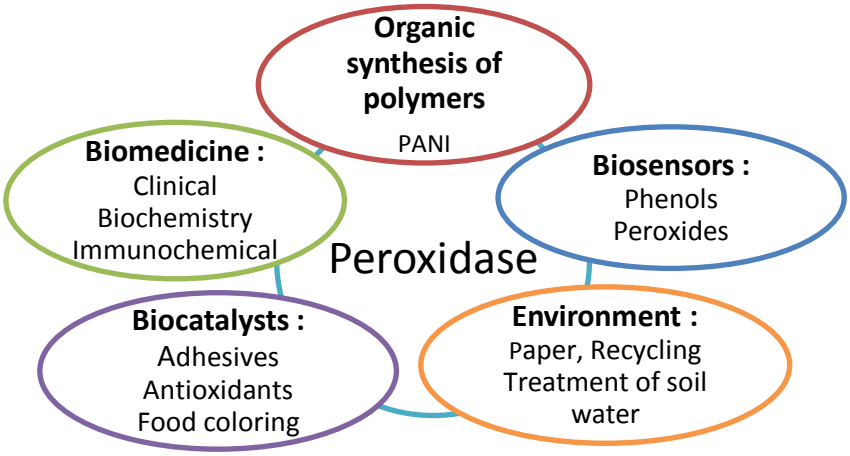

Figure 6 – *Schematic representation of biotechnological applications of peroxidases.*

i) Biocatalysts

Peroxidases are nowadays used as biocatalysts for decoloration of synthetic dyes and in the treatment of soil and water [15]. Dyes are used in paper, textile and others industries. Their processing generates a large number of phenolic compounds, which are highly toxic and sometimes carcinogenic, so they must be removed before the waste is discharged into the environment [16]. For their removal nowadays exist a high number of processes but even if they are effective, they often have high costs, limited applicability, high energy expenditure and/or may lead to generation of a series of products that are also harmful to the environment. The use of peroxidases may have a significant potential, due to their high versatility in oxidizing even inert compounds amenable to chemical waste treatments [17].

ii) Biosensors

Peroxidases can be used in the construction of enzyme-based biosensors for detection of different compounds. These biosensors are highly valuable in biomedicine. For example, HRP based devices are employed as diagnostic kits for measuring uric acid, glucose, cholesterol, triglycerides and ascorbic acid in biological fluids [18]. For example, the kit for cholesterol determination relies on an enzymatic colorimetric method, which is precise, quick and selective. This method uses: cholesterol oxidase, cholesterol esterase and HRP immobilized on matrix. If the peroxidase is immobilized on a conductive support material such as carbon, graphite or gold, a direct electron transfer (ET) between the electrode surface and the active site of the enzyme can take place. Thus, the immobilized enzyme on the electrode can be oxidized by hydrogen peroxide and then reduced by electrons from the electrode. If the employed peroxidase is glycosilated direct ET becomes unfavorable, because of decreased affinity between the support material and the protein and typically long ET distances [19]. Peroxidase biosensors based on direct ET are nowadays used to detect H_2O_2 and small amounts of organic hydroperoxides [19].

Recently, it was reported that the concentration of substrates such as glucose, alcohols, and others molecules can be determined via direct ET between immobilized peroxidase and electrode [19]. ET between the enzyme and the electrode can also be mediated. Mediated ET is typically more effective than direct ET. In this manner various unfavorable factors such as: long distance of ET between the electrode surface and the enzyme active center, the heterogeneous orientation of the enzyme on the electrode or low adsorption of the enzyme due to the large percentage of glycosylation are avoided [19]. Nervertheless, some disadvantages, most often related to interference of employed mediators can be associated with this approach.

2.1.5. Dye decolorizing Peroxidases

DyPs were discovered about 10 years ago when DyP was isolated from the fungus *Thanatephorus cucumeris Dec 1*[5]. They are capable of degrading anthraquinones (AQs), a class of dyes that are widely used in industry [15]. In addition, DyPs can efficiently degrade numerous organic and inorganic coumponds, such as: typical peroxidases substrates, azo dyes and phenol derivatives [20]. This process is very important for the environmental decontamination. DyPs take the hydrogen from hydroxyl groups of dyes and generate radical compounds, then the radical reaction continues and the dyes are degraded or polymerized into other less harmful molecules. In animals, the connection between DyPs and several diseases have been intensively studied, mainly, the role of peroxisomes in aging and several neurodegenerative diseases, such as Alzheimer and Parkinson [5]. In plants they might promote the removal of H_2O_2, thus protecting against xenobiotics. Due to their relatively recent discovery, physiological and mechanistic features of DyPs from different organisms still require further studies. However, it appears that their physiological role strongly depends on their origin.

- **Specific features**

As mentioned before, DyPs are heme peroxidases, however, they have several characteristics that distinguish them from all other peroxidases, including high substrates specificity, a lack of homology to most of other peroxidases, and the ability to function very well under lower pH conditions compared to all other plant peroxidases [21]. Some peroxidases have the sixth axial site occupied by a weak ligand (i.e. H_2O) but in DyPs studied so far, the heme iron is pentacoordinated. In its fifth (proximal) axial position, a conserved His is present while the typically distal His is absent. This feature is very important to the catalytic activity because this position remains free for the H_2O_2 ligation [21]. The conserved Asp most likely acts as a proton donor/acceptor and takes the place of the catalytic His present in plant peroxidases. This substitution possibly accounts for high activity of DyPs at low pH values [7].

Crystal structure of DyP from *Bjerkandera adusta* presented by Yoshida (DOI:10.2210/pdb2d3q/pdb) shows two domains, each one adopting a ferredoxin-like fold [RSCB PDB]. The structure reveals one single motif, with two sets of anti-parallel β-sheets between α-helices above the distal area of the heme. The analysis of RCSB PDB shows that there are only few structures of DyP's reported until today, for example, DyP from *T. cucumeris Dec 1*, DyP from *Rhodococus jostii RHA 1*, TyrA from *Shewanella Oneidensis,* DyP from *Bjerkandera adusta* and DyP from *Bacteroides thetaiotaomicron VPI- 5482* [RSCB PDB]. The comparison of these structures reveals that the residue next to the Asp in the distal area and next to the proximal His (Fig. 7) can be different in DyP´s from different organisms.

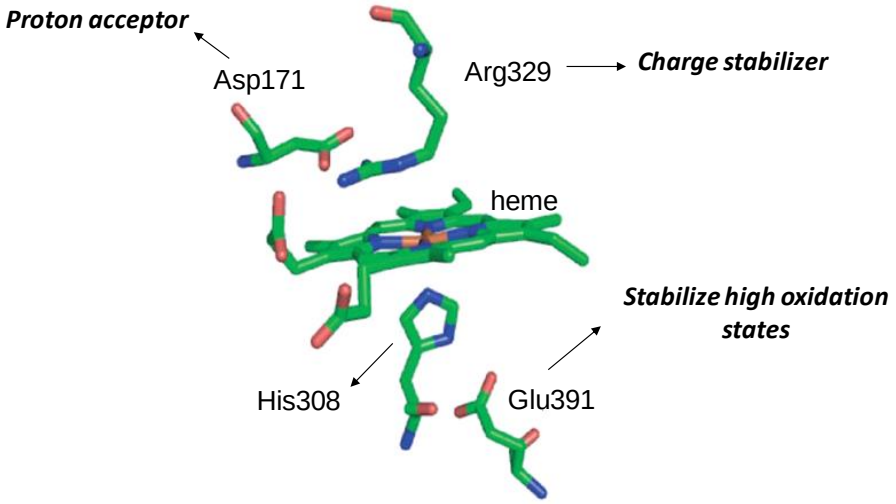

Figure 7 – *Schematic representation of the active site of DyP from Tanatephorus cucumeris Dec 1 [22].*

The distal area of DyP from *Tanatephorus cucumeris Dec 1* contains the amino acid Arg, while the DyP from other organism can possess an Asn, but both play the same role, acting as a charge stabilizer during the catalytic reaction. In the proximal area Glu stabilizes high oxidation states, such as Co I, by forming a hydrogen bond with the proximal His (His308 in *T. c. Dec I*). The catalytic mechanism is not clearly understood, however, it likely follows the same mechanism of plants peroxidases, as proposed by Sugano [22]. When Asp171 acts as proton acceptor and Arg329 as charge stabilizer, in the next step Asp acts as acid-base catalyst and H_2O_2 is heterolytically cleaved, resulting in Co I.

The DyP-type peroxidase family is clearly a unique heme peroxidase family. DyPs show several configurations, for example TyrA is a dimer, where BtDyP assembles into a hexamer. Structural and sequence comparisons of DyPs with other heme peroxidases demonstrate a conservation of heme-binding residues, including an absolutely conserved His (His170 in HRP, His173 in MnP or His226 in DyP from *Rhodococus jostii RHA1*). Several x-ray structures reveal the presence of calcium ions or glycans. The primary and tertiary structures of DyP family are different from those of other heme peroxidases and it is a big challenge to understand which mechanistic and physiological implications these differences have.

2.2. Characterization of stability of proteins

Proteins are natural macromolecules having, in general, a fixed composition and an ordered structure, which rely on their native structure for executing their respective functions. This conformation is called the native state and it is present when the macromolecule is in thermodynamic conditions similar to the physiological environment. Immobilized enzymes, with a promising biotechnological role are very attractive objects of study. An aspect to be taken into account during the immobilization of proteins is that immobilization under certain conditions can induce denaturation [12]. In general, changes in environment can cause a loss of 3D structure of protein, and this denaturation may be due to several factors, such as a variation of pH, temperature or denaturing agents such as urea or GndHCl. This denaturation can be: i) reversible, when the protein regains its native state after eliminating the cause of the denaturation or ii) irreversible, if the protein loses its 3D structure, compromising its biological function [23]. The detection and characterization of intermediate states during denaturation is a fundamental aspect in the study of protein folding, since it is well recognized that proteins adopt a number of intermediate forms before reaching their functional native structure. The best known intermediate is "molten globule". It is characterized by a fairly ordered secondary structure in a compact form comparable to that of the native protein and well-defined tertiary structure. Dominant forces in protein folding are hydrophobic effect and hydrogen bonding, and the most destabilizing force is the conformational entropy. The folded state is stabilized by the fine packaging of peptide bonds and side chains of non polar residues. The native state (N) is slightly more stable than the unfolded state (U) under physiological conditions (2-10 kcal mol^{-1}) [23].

2.2.1. Denaturation induced by pH

Most proteins are denatured at extreme pH values. The protein denaturation occurs because they have many acidic or basic groups and pH changes lead to a state in which the folded protein is no longer stable [24]. The pH increase can result in the loss of protons in the side chains of amino acids such as Lys, Tyr, His, Arg and Cys. Conversely, a decrease in pH causes protonation of carboxyl groups of the side chains of amino acids like Asp and Glu. These alterations of the degree of protonation of the amino acids change the electrostatic interactions (salt bridges) and the hydrogen bonds that exist at physiological pH values. The pH also effects on enzyme activity by changing the ionic form of amino acids of the catalytic center (affecting the catalytic constant, k_{cat}). Measuring enzyme activity at different pH, yields the enzyme stability curve as a function of pH [24].

2.2.2. Reversible thermal denaturation

When denaturation process takes place in equilibrium, it is necessary to assume a model, which can be used to determine relevant thermodynamic parameters [23]. In the thermal denaturation of many small globular proteins, it was observed that there are only two significantly populated states: the native state (N) and the denatured state (D). The unfolding of these proteins is described quantitatively by the equilibrium model of two states:

$$N \rightarrow D \qquad (1)$$

The thermodynamic parameters, enthalpy (ΔH^{D}_{N}), entropy (ΔS^{D}_{N}) and Gibbs free energy (ΔG^{D}_{N}) are calculated as follows:

$$\Delta H^{D}_{N} = H(D) - H(N) \qquad (2)$$

$$\Delta S^{D}_{N} = S(D) - S(N) \qquad (3)$$

$$\Delta G^{D}_{N} = G(D) - G(N) \qquad (4)$$

The denaturation temperature ($T_{1/2}$) is defined as the temperature at which exists the same amount of protein in native and denature state, X_D = 1/2. In a process of two-state denaturation of a monomeric protein, predicted transitions are almost symmetrical and the value of calculated $T_{1/2}$ is close to the temperature corresponding to maximum heat capacity (T_m) [23].

2.2.3. Denaturation induced by chemical agents

Conformational stability of a protein can be probed through the study of reversible chemical denaturation, using denaturing agents such as guanidine hydrochloride (GndHCl) or urea [23]. For that propose one typically measures changes of some spectroscopic properties such as fluorescence at different concentrations of denaturing agent [23]. The intrinsic fluorescent probes of protein are the aromatic amino acids (Trp, Tyr and Phe). Equilibrium constant (K_D), and free Gibbs energy (ΔG °) can be expressed by:

$$K_D = (y_N - y)/(y - y_D) = \exp(-\Delta G°/RT) \quad (5)$$

where y_N and y_D are the values of fluorescence of native and denatured protein respectively, and R the gas constant.

Representing ΔG ° as a function of the concentration of denaturing agent, allows for determination of the Gibbs free energy in the absence of denaturing agent:

$$\Delta G° = \Delta G° (H_2O) - m\,[GndHCl] \quad (6)$$

where ΔG ° is the Gibbs free energy in equilibrium and ΔG ° (H_2O) in the absence of denaturing agent (parameter indicating protein stability); [GndHCl] is the concentration of denaturing agent and m is a proportionality constant that is related to the change of nonpolar area exposed to the solvent, associated with denaturation [23]. Concentration of denaturing agent at which there is the same number of molecules in the native and denatured state ($D_{1/2}$) can be expressed by:

$$[D_{1/2}] = \Delta G° (H_2O)/m \quad (7)$$

Depending on the excitation wavelength, the aromatic amino acids contribute to the fluorescence emission spectrum to different extent. Thus, if excited at 280 nm, both Trp and Tyr will contribute, however, when excited at wavelengths above 295 nm, only fluorescence emitted from Trp will be detected [23]. The denaturation of proteins generates a fluorescence emission spectrum that can have more or less intensity than the protein in native state, but the wavelength of maximum emission always evolves in a predictable increase in value. Thus, the spectrum provides information on changes in the environment of the fluorophore. The peroxidases are enzymes in which the heme prosthetic group acts as a "quencher" of fluorescence in the native protein. However, when the protein is denatured, the fluorescence intensity undergoes a significant increase, caused by the reorientation of Trp relatively to the heme [24].

2.3. Spectroscopic analysis of heme proteins

2.3.1. Electronic configuration and UV-Visible spectra of heme proteins

Absorption spectra of metalloporphyrins contain an intense band at 400 - 450 nm ($\varepsilon \approx 10^5$ $M^{-1}cm^{-1}$) called Soret band and weaker bands at 550 - 600 nm ($\varepsilon \approx 10^4$ $M^{-1}cm^{-1}$), which are called the Q bands [25]. The position of these bands is influenced by the metal oxidation state, metal coordination, spin state, and the protoporphirine substituents (i.e. type of the heme). All absorption bands are associated with π-π* transitions of the heme cofactor. The Soret transition is strictly allowed, while the Q bands are only partially allowed, as well as the charge transfer bands at 630 – 650 nm (present in Fe^{3+} 5cHs species) [25]. Molar absorption coefficients of the Soret band and its position depend on the oxidation state of iron. When iron is pentacoodinated (Fe^{3+}) is 105±6 when is hexacoordinated (Fe II) is 177±9 $mM^{-1}cm^{-1}$, Soret band of the ferric protein is downshifted in respect to that of the ferrous protein [26].

In Co I, heme is oxoferryl with a Soret band with an intensity that is half the one of the resting state, centered at 403 nm. Usually the Co I is unstable and spontaneously reacts back after few minutes. The Soret band of Co II is shifted to 420 nm, with intensity comparable to that of the resting enzyme, in addition a double peak, with maxima at 527 and 554 nm is present in the spectra [27].

Some earlier studies have demonstrated a presence of compound 0 (Co 0), before the formation of the Co I, at lower temperatures, in which Fe (III) binds to a hydroperoxide [22]. UV-Visible spectroscopic fingerprints of different intermediates including Co III (hybrid of resonance of Fe (III)-superoxyde and Fe (II)-dioxygen) are summarized in Table 1.

Table I – *Visible of HRP and several other representative peroxidases, adopted from literature [28].*

	HRP		Cytochrome P450		Catalase	
	Soret	Other UV-Vis features	Soret	Other UV-Vis features	Soret	Other UV-Vis features
Resting state	404	610, 642	424	539, 574	405	504, 538, 640
Co 0	410	330	---	---	---	---
Co I	400	577, 622, 651	367	694	405	660
Co II	420	527, 554	420	----	429	536, 568
Co III	417	544, 580	---	---	---	---

2.3.2. Raman Spectroscopy

Raman spectroscopy is vibrational spectroscopy. It probes vibrational energy levels within a molecule. The molecular structure, types of atoms and bonds, molecular geometry and hydrogen bonding affect the vibrational spectra. Therefore Raman spectra provide a characteristic "fingerprint" of the molecule structure. Raman spectra are usually presented with the y-axis values representing of the relative intensities of Raman bands and the abscissa the values of the Raman shifts in terms of wave numbers [29].

The atoms present in a molecule are constantly oscillating even at very low temperatures. In fact, even in solids at temperatures near absolute zero, the atoms are continuously oscillating around the equilibrium position. A molecule with N atoms that are free to move in three dimensions has 3N degrees of freedom, of which three degrees correspond to the translational movements of the molecule. For a nonlinear molecule there are three degrees of freedom for rotation. The other (3N-6) degrees of freedom are for the vibrational movement of the molecule [30]. For linear molecules there is no rotation around the internuclear axis and, consequently, there are (3N-5) degrees of freedom for the vibration. These degrees of freedom (i.e. 3N-6 in non-linear and 3N-5 in linear molecules) are referred to as normal modes [30].

When, a monochromatic radiation of frequency, ν_0, is focused on a cell containing a transparent substance most of the radiation passes through it without changes. However a small fraction of the radiation (~ 0.1%) is scattered by molecules in the sample in all directions. Inelastic scattering ($\nu_0 + \nu_1$) and ($\nu_0 - \nu_1$) is known as Raman scattering [31]. The lines of lower frequency than the incident ($\nu_0 - \nu_1$) are known as Stokes lines and lines of higher frequency ($\nu_0 + \nu_1$), are called anti-Stokes lines. The intensity of Stokes lines is always higher than anti-Stokes lines, because the population of the vibrational ground level is always higher.

The frequency change is also called "Raman shift":

$$\nu_0 - \nu_{Raman} = \text{Raman shift} = \Delta\nu$$

The fraction of Raman scattering (inelastic) is about 10^{-7} of the incident intensity. In fact, the Raman effect is very weak, which requires the use of monochromators in order to keep the "stray light" at very low level, because otherwise, the Raman scattered light is masked. It is also necessary to use sensitive detectors and efficient optical systems to guide the laser light to the sample and scattered light to the detector.

- **Small molecules versus proteins**

The size of the biological systems that are probed by vibrational spectroscopy in the life sciences can vary substantially. They range from small molecules, building blocks of biopolymers or cofactors of proteins up to protein assemblies, membranes, or DNA-protein complexes. Concomitant with the increasing size of the system, the number of vibrational modes, and therefore signals in the spectrum increases. For instance, small molecules with less than 50 atoms, will give origin to ca.150 normal modes. It is usually impossible to resolve all the individual vibrational bands [11]. For biopolymers such as proteins, the number of vibrational modes is relatively large, resulting in complex spectra with many overlapping bands of slightly different frequencies. So, it is not obvious, how detailed information, for example, on the interaction of a substrate in the catalytic centre of an enzyme, or on the minute structural changes occurring in the protein during the enzymatic process, can be derived from vibrational spectra of large biological systems [11].

This problem can be overcome in metalloproteins, if the wavelength of the monochromatic light, which is used to excite the sample, is selected to coincide with an electronic transition of a chromophoric group of the protein. Under these resonance conditions, the probability of the scattering-induced transitions, and thus the intensity of the Raman scattered light originating from vibrational modes of the chromophore, is selectively enhanced by several orders of magnitude [31]. Under these conditions the resonance Raman (RR) spectrum displays the vibrational bands of the chromophore exclusively, whereas the Raman bands of the protein matrix remain invisible. This selectivity is associated with an enhanced sensitivity, thus the protein concentration required for high quality spectra is drastically reduced. Raman spectroscopy has advantages and disadvantages for the study of biological molecules. Amongst the advantages is the ability to study in situ aqueous systems. One of the disadvantages is that using highly focused beams, sensitive biological molecules and tissues can in some cases be damaged [31]. Nowadays Raman spectroscopy and imaging are becoming useful techniques in medicine, capable of distinguishing between healthy and cancerous tissues, as well as benign and malignant tumors [31].

2.3.3. Resonance Raman of heme proteins

Resonance Raman spectroscopy is a technique with much higher sensitivity than conventional Raman spectroscopy. It is especially useful in the studies of metallo-enzymes, including heme, copper and non-hemic iron proteins. RR allows for increased selectivity, providing information on chromophore only [32]. For instance, information on the coordination geometry of the metal and the ligand environment and structural features of catalytic intermediates of heme enzymes in particular, can be specifically addressed.

RR spectra of heme proteins/enzymes are most informative upon excitation into Soret band of electronic absorption spectra of the porphyrin using the 413 nm line of a Kr^+ laser. Among others, the spectra show the core-size marker bands in the 1300 - 1700 cm^{-1} region, sensitive to the redox, spin state and coordination of the heme iron [31].

Heme iron is in a d^5-electronic configuration in an octahedral ligand field, for which the five d-orbitals can split into three degenerate e_g- and two degenerate t_{2g}-orbitals [31]. This splitting results in two different possibilities for distributing the five d-electrons of ferric heme, on one hand all electrons are paced into the three e_g-orbitals, such that only one

electron remains unpaired (low spin, LS, S = 1/2) on the other hand, each electron can be placed into an individual orbital corresponding to the high spin (HS, S = 5/2) configuration (Fig. 8). Some proteins were shown to be able to form an unusual heme spin state, a quantum mechanically mixed-spin state (QS). The QS heme state results from the admixture of HS and intermediate spin (IS, *S* = 3/2).

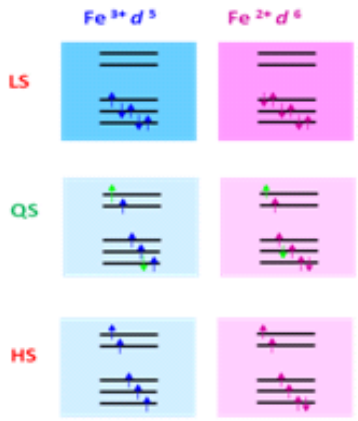

Figure 8 – *Schematic representation of LS, HS, and QS heme electronic configuration [33].*

If two strong axial ligands are coordinated to the heme iron, the energy gap between the orbitals become larger, making doubly occupied orbitals an energetically favored configuration (i.e. six-coordinated LS, 6cLS). Weak ligands originate a six-coordinated HS (6cHS) configuration, which is also obtained when the heme iron is coordinated by only one axial ligand (five-coordinated HS, 5cHS) [31].

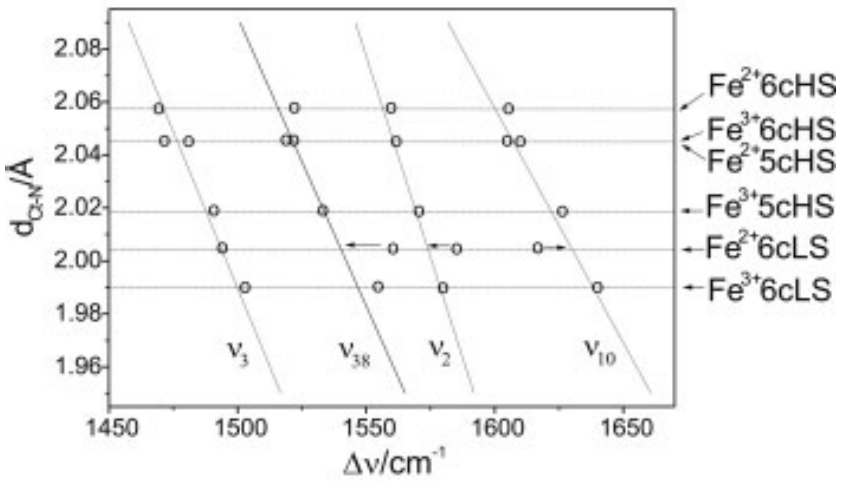

Figure 9 – Correlation between the porphyrin core size and the frequencies of selected heme modes for iron porphyrin complexes [31].

For heme proteins the study of the marker bands between 1300 and 1700 cm^{-1} allows a determination of the oxidation, spin, and coordination state of the heme iron [31]. These marker bands are correlated with different state of heme iron, for example the v_4 mode responds specifically to changes in the oxidation state of the heme iron. In ferric hemes it is typically found between 1370 and 1375 cm^{-1} but it is lowered to 1358–1363 cm^{-1} in the ferrous state. The v_2 and v_3 modes are mainly sensitive to changes in the coordination pattern and spin state [31].

2.3.4. Surface Enhanced Resonance Raman Spectroscopy of Immobilized Heme Proteins

Surface enhanced resonance Raman (SERR) spectra are obtained from samples that are adsorbed on certain rough metal surfaces (usually silver, copper or gold) [2]. For SERR effect to occur, three conditions have to be simultaneous fulfilled: electronic transition of the sample has to coincide with energy of the exciting laser line (resulting in RR effect) and in addition, this energy has to match the energy of surface plasmons of the metal support [2].

When these three conditions are met, enhancements of 10^8 can be achieved for molecules adsorbed onto nanoscopically rough surface. For example, Soret band excitation with 413 nm laser of heme proteins adsorbed on nanostructured silver (surface plasmon energy ~ 400 nm) provide superior selectivity and sensitivity. The metal that gives origin to SER effect can furthermore serve as a working electrode in spectroelectrochemical studies, providing important insights into redox properties of heme proteins immobilized on biocompatible metal electrodes. The metal can be chemically functionalized with SAMs (self assembled monolayers) to facilitate absorption of biomolecules under preservation of their native structure [34]. Coupled with electrochemical methods SERR spectroscopy can provide unique information on electron transfer processes in immobilized proteins.

Moreover, SERR is the only available approach that can provide simultaneous insights into structural and mechanistic features of immobilized heme enzymes that are employed in construction of bioelectronic devices.

- **Techniques for immobilizing enzymes**

Immobilization of proteins for biotechnological applications requires essentially the unchanged native structure. The enzyme must be immobilized on the surface maintaining its catalytic activity. Besides, the diffusion of substrates and products to and from biocatalytic interface should be possible. The ideal support for the immobilization of enzymes should be insoluble in water, chemically inert and connectable easily to the enzyme. The most common methods for immobilization of enzymes are via encapsulation (microspheres or polymer matrix) or by ligation of the enzyme to the support (Fig. 10). The choice of the immobilization method depends primarily on the enzyme and the support to be used in making the biosensor and/or biocatalyst [35].

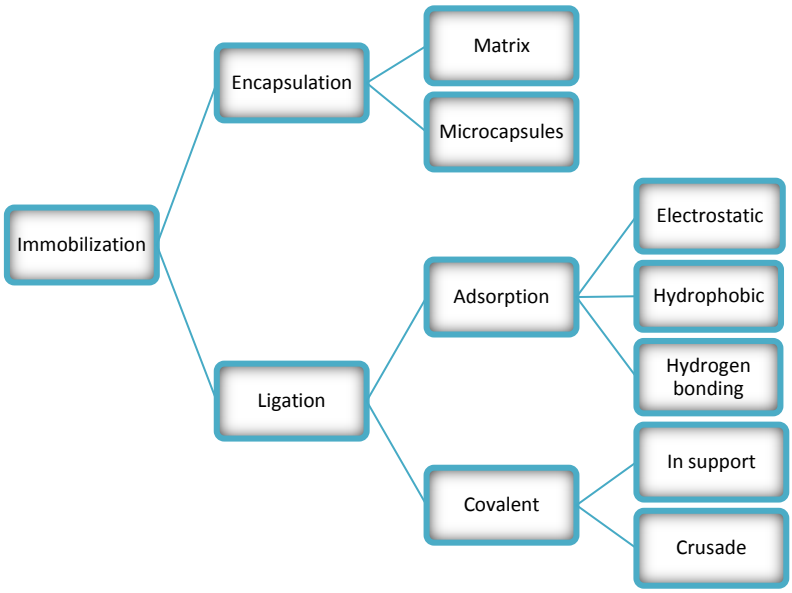

Figure 10 – *Principal methods for the immobilization of enzymes.*

Encapsulation is suitable for almost all kinds of enzymes but among its major disadvantages, which makes it less popular, are: steric restrictions, modifications of protein structure and uncontrollable diffusion of the protein through the matrix.

- **Self Assembled Monolayers (SAMs)**

The interaction between proteins and surfaces of noble metals can occur through non-covalent bonds (Fig. 11) (electrostatic, hydrogen bonding) or covalent bonds. This ligation occurs typically by cross-linking between functional groups of the protein and the surface [36]. Enzymes are linked to the solid support through functional groups present in their amino acids, the main amino acids used for covalent binding are Lys and Cys.

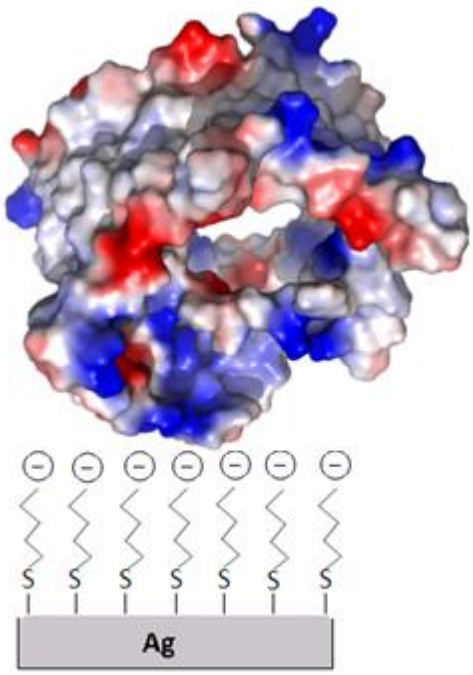

Figure 11 – *Schematic representation of electrostatic interaction between SAM and a protein with positively charged patch on a surface.*

Common approach for protein immobilization relies on use of SAMs, which provide a well-defined organic platform with controllable chemical functionalities and specific binding of biomolecules [36]. The applications of SAMs are widespread in fundamental and applied science.

SAMs (Fig. 12) of ω-functionalized alkanethiols form organized layer of molecules. They are commercially available with typically 2 to 16 CH_2 groups acting as spacers. The thiol headgroup has specific affinity to nobel metals and forms stable covalent bonds with it.

On the other end, SAMs have a functional group, such as: cationic, anionic or neutral (or specifically designed, for instance, carrying DNA, for immobilization of DNA binding proteins), to which protein can bind [2].

Depending on surface charge distribution of the particular protein (Fig. 11), appropriate SAM functional group(s) are chosen to provide biocompatible surface for protein immobilization.

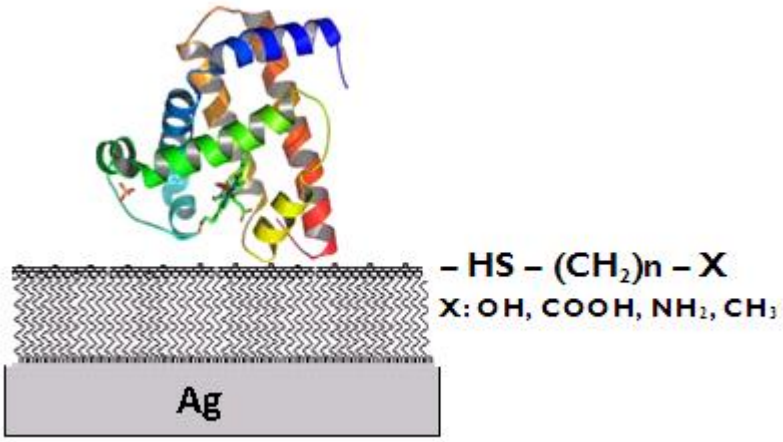

Figure 12 – *Schematic representation of protein immobilization on SAM coated to the surface.*

SAM acts as "barrier", preventing a direct contact between protein and metal (bare solid support), which could lead to conformational changes or denaturation of proteins [2]. The distance between the metal and the protein can be varied using SAMs at different chain lengths (Fig. 12). The success of wide utilization of the SAMs is due to several factors, such as easy preparation, their stability, reproducibility and reliability of the formed surfaces, as well as the possibility of applying a variety of techniques for their characterization.

2.3.5. Biomedical applications

Conventional Raman spectroscopy is useful for studying secondary structure of proteins and nucleic acids. The development of near-infrared Raman spectroscopy (FT Raman) has widen interest in the use of Raman spectroscopy in medical diagnostics. Typically such applications rely on the differences in lipid/protein ratios in normal and cancerous tissue. Composition changes are reflected in the fingerprint region and in the C-H stretching

region. Raman spectroscopy is non destructive and therefore attractive for biomedical applications both *in-vivo* and *in-vitro*.

Raman spectroscopy is nowadays routinely used in hospitals as a powerful diagnostic tool, especially for surface (skin) cancers. With a help of optical fiber probes, application of Raman spectroscopy is extended to internal organs and tissues. It is also nowadays a valuable complementary tool to histological analysis, for characterization of biopsy samples [5].

3.1. Enzyme purification

DyP-type peroxidase from *Pseudomonas putida* was heterologously overexpressed in *E.coli* and purified according to the following steps:

- Enzyme production
    - Transformation of the expression vector containing the recombinant gene into an *Escherichia coli* strain (Appendix I).
    - Growth at 37°C, in Luria Bertani (LB) broth supplemented with ampicillin and hemin, induction for the gene expression with isopropyl-β-D thiogalactopyranoside (IPTG).
    - Cell harvesting by centrifugation after 24h of growth.
    - Cell disruption in the French pressure unit.

- Purification by liquid chromatography
    - Anionic exchange
    - Size exclusion
    - Electrophoresis (SDS-PAGE) to monitor the sample purity (Appendix II)

- Protein quantification

- Biochemical characterization

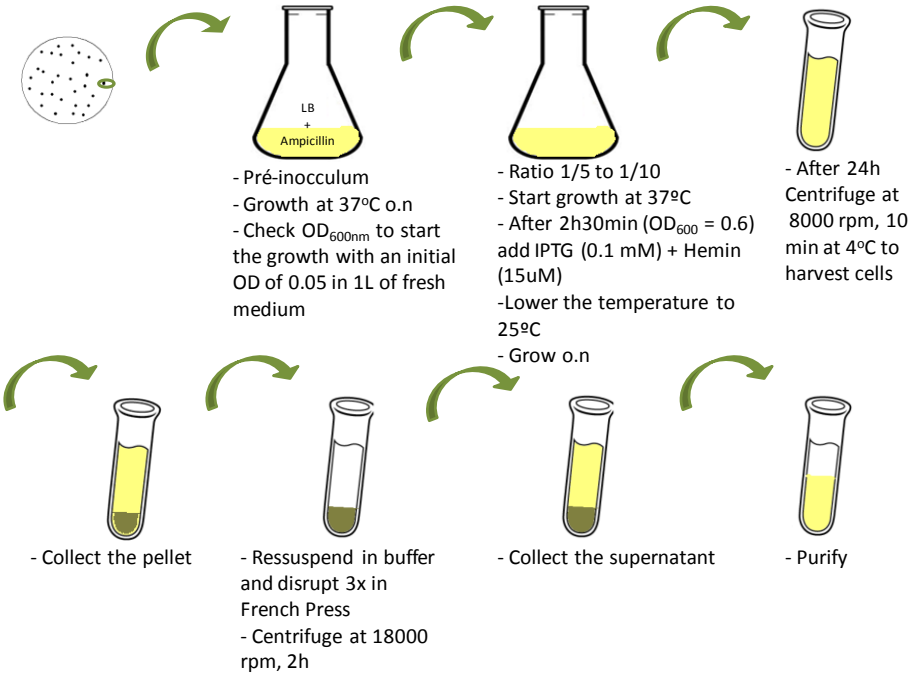

Figure 13 – *Schematic representation of purification steps of DyP-type peroxidase from Pseudomonas putida.*

3.1.1. Cloning and expression of DNA fragments of PpDyP

After PCR amplification, the recombinant gene was digested with *Nde*I and *Bam*HI and inserted between the respective restriction sites of plasmid pET-21a(+) to yield pRC-1. Then was introduced into the host expression strain *E. coli* BL21* in which the PpDyP protein was produced under the control of the T7*lac* promoter. The recombinant strain was grown in LB medium (Appendix III) supplemented with amplicillin (100 μg mL^{-1}) at 37°C.

Growth was followed up to an OD_{600} of 0.6, at that point 100 μM isopropyl-β-D-thiogalactopyranoside (IPTG) and 15 μM hemin were added to the culture medium. Then the temperature was lowered to 25°C, and incubation was continued overnight. Cells were harvested by centrifugation (8,000 rpm, 10 min, 4°C).

3.1.2. Purification by liquid chromatography

After cell harvesting, cell sediment was suspended in 20 mM Tris-HCl buffer (pH 7.6), containing DNase I (10 μg mL^{-1} extract), $MgCl_2$ (5 mM) and a mixture of protease inhibitors, antipain and leupeptin (2 μg mL^{-1} extract). Cells were disrupted in a French press and cell debris was removed by centrifugation (18,000 rpm, 2 h, 4°C). Supernatant was used for protein purification.

All buffers used for chromatography were made with MilliQ water, filtered with 0.22 μm filters and degassed under vacuum by extraction.

- **Anionic exchange chromatography**

FPLC (Fast protein liquid chromatography) was carried out at room temperature. A Q Sepharose column (commercially packed), glass column (1 cm x 30 cm) with 12 cm^3 of DEAE-Toyopearl 650M (average particle size of 40-90 μm and pore diameter of 1000 A) was used. Positively charged resin with remains of diethylaminoethyl ($^{-}O\text{-}CH_2\text{-}CH_2\text{-}HN^{+}\text{-}(C_2H5)_2$) binds proteins that are charged negatively. An equilibration buffer 20.0 mM Tris-HCl pH 7.6 was used and a flow rate of 3 mL min^{-1} was employed. Elution was performed with 20 mM Tris-HCl at pH 7.6 and 1 M NaCl, with a linear gradient of NaCl and a flow rate of 1 mL min^{-1}. 3 mL fractions were collected and concentrated with an Amicon cell (membrane of 30 kDa) before passing to the next column in a centrifuge at 3000 rpm and 4 °C for 30 min.

- **Size exclusion chromatography**

Size exclusion chromatography was carried out at room temperature. A stationary phase Superdex 200 HR 10/30 column (commercially packaged). Agarose and dextran matrix with a pore size of 13 μm, working pH range between 3 and 12, and optimal separation range between 10 and 600 kDa) was used. It was equilibrated with buffer 20 mM Tris-HCl pH 7.6 over night. The flow rate was 1 mL min^{-1}. The sample obtained after this chromatographic step was concentrated in an Amicon cell (membrane of 30 kDa). Centrifuged at 3000 rpm at 4 °C for 20 min.

- **Purity analysis by polyacrylamide gel electrophoresis**

The procedure used for electrophoresis is the folowing:

- Mix the samples with protein Loading buffer and boil for 5 minutes at 96ºC.
- Mount plates - Mini protean III - Bio Rad.
- Prepare the gel solution and apply it to the desired level (at least 0.5 cm below the comb). Apply Butanol to remove the air bubbles.
- After polymerization, remove all Butanol with Milli-Q water and dry with filter paper.
- Apply the gel to the top packaging and insert the comb.
- Assemble the apparatus containing the electrophoresis running buffer.
- Perform electrophoresis (100 V to 200 V).
- Subject the gel to Western blot assay or stain it with Coomassie blue for 30 minutes at room temperature followed by treatment with bleach.

Composition of each solution used in this step is described in Appendix III.

- **Determination of protein concentration**

To determine the concentration of protein in solution we employed the Bradford method. We followed the absorbance of a colored compound which is formed from the protein and Bradford reagent. First we constructed a calibration curve from a solution of 1 mg ml^{-1} BSA (M = 66 kDa, ε_{280} = 43824 M^{-1} cm^{-1}), with amounts of BSA ranging between 0 and 60 μg (0-60 μL). Once constructed the calibration curve is used for reading the unknown concentration of protein of interest. 20 μL of each protein sample was added and was brought to a final volume of 1020 μL by adding 1000μL of Bradford reagent, than shaken and incubated for 10 min at RT. After that time, we proceeded to read the absorbance at 595 nm.

3.2. Biochemical Characterization

3.2.1. Molecular mass determination by molecular exclusion chromatography

The molecular mass of PpDyP was determined by a gel filtration Superose 12 10/300 GL (GE Healthcare Bio-Sciences, Sweden) column equilibrated with 20m MTris–HCl buffer, pH 7.6, containing 0.2 M NaCl at a flow rate of 1 ml min^{-1} in $AKTA_{FPLC}$. Thyroglobulin (670 kDa), γ- globulin (158 kDa), ovalbumin (44 kDa), myoglobin (17 kDa), and vitamin B12 (1.35 kDa) were used as standards (Bio-Rad Laboratories). The procedure is described in Appendix IV.

3.2.2. Denaturation induced by pH

Dependence of purified PpDyP activity on pH in the range between 3 and 10 was recorded by monitoring the oxidation of ABTS as substrate at 420 nm using a Nicolet Evolution 300 spectrophotometer from Thermo Industries (Waltham, MA, USA).

3.2.3. Reversible thermal denaturation

Temperature profile in the range between 10 and 40°C was measured by monitoring the ABTS oxidation at 420 nm (ε = 36000 $M^{-1}cm^{-1}$) in the presence of 0.2 mM H_2O_2. The effect of temperature on the PpDyp stability was determined by incubating the enzyme in 20 mM Tris-HCl with 0.2 M NaCl, pH 7.6 or in 20 mM sodium acetate buffer, pH 5.0, during 1 h at different temperatures. The enzyme was submitted to a temperature increase at a rate of 1°C/min until 100°C.

3.2.4. Denaturation induced by chemical agents

To carry out these experiments, we measured unfolding of PpDyP reflecting exposure of the Trp residues using a Carry Eclipse spectrofluorimeter at excitation wavelengths of 280 nm and 296 nm and emission wavelength of 330 nm. To induce protein unfolding we used guanidinium hydrochloride (GndHCl). We mixed different volumes of standard solution (GndHCl 7.5M) in a phosphate buffer at pH 7.6, to obtain final concentration in a range between 0 and 4,5 M, while keeping protein concentration constant. The changes were recorded at 296 nm, 25 ° C.

3.3. Spectroscopy

3.3.1. UV-Visible spectroscopy

Resting state ("as purified") PpDyP spectra were recorded from Nicolet Evolution 300 spectrophotometer from Thermo Industries (Waltham, MA, USA) using 50 μM of protein in the 300 – 700 nm range, at RT. Reduction of the protein was achieved by addiction of a small amount of solid sodium dithionite (2-5 mg) and measured under the same conditions.

3.3.2. Raman Spectroscopy

- **Instrumentation**

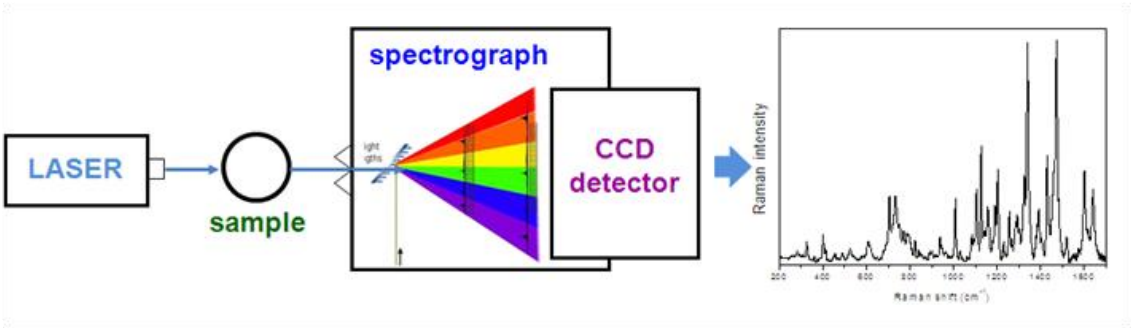

Figure 14 – *Schematic representation of a basic system for Raman spectroscopy.*

The basic system for Raman spectroscopy can be divided into three main parts: the excitation source, capture and signal filtering, and handling/storage of the signal. The first part of the system refers to the source to excite the sample, which comprises a light source (laser), and are some optical elements (lenses, mirrors), responsible, for focusing and directing the laser beam to the sample [31].

The second part of the system corresponds to the optical components (microscope), responsible for capturing and filtering the signal scattered by the sample. The major part of

the incident light is elastically scattered by the sample. A small portion of the scattered light that carries the information about the sample is filtered and guided into the spectrometer. Then it is focused onto the entrance the spectrophotometer, and further onto a system of internal diffraction gratings that separates the signal spread in its main components, and finally to the detector (charge coupled device - CCD). The data are then processed by the computer [31]. They can be subjected to component analysis performed by specific software and/or stored for future analysis. In this work we used Jobin Yvan U1000 Raman spectrometer equipped with a doubled monochromator 1200 m/l grating and ligand N_2 cooled CCD. In all studies 413 nm laser light was provided by Kr^+ (Coherent Innova 302) laser.

3.3.3. Resonance Raman

For RR experiments we used a cylindrical quartz cell (Helma) (Fig. 15), placed onto a rotating holder. Due to the rotation, the liquid sample is pressed against the wall of the cell forming a film, onto which the laser beam is focused by Nikon 20x objective. We used typically 60 - 120 μL of 128 μM of sample. The Raman spectra were measured with a Kr^+ laser (Coeherent Innova 320) line of 413 nm and power of 2-4 mW in the sample. LabSpec software was used for data acquisition and simple manipulation. Prior to measurements, laser beam power was adjusted by power meter, the spectrum was calibrated by the strong mercury line at 435.833 nm and the light was carefully focused onto the sample to ensure maximum signal intensity.

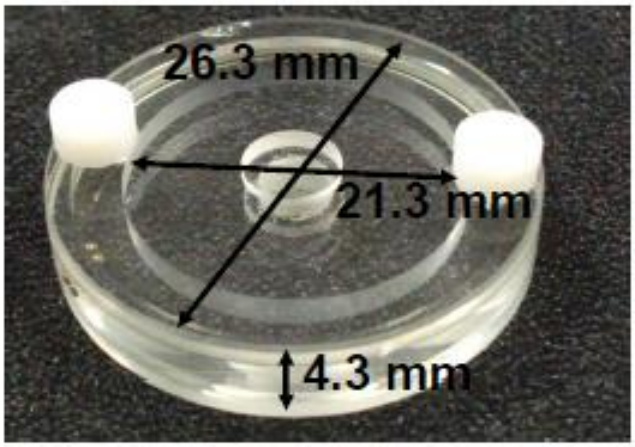

Figure 15 – *Cylindricall quartz cell (Helma) [37].*

3.3.4. Surface Enhanced Resonance Raman

For SERR experiments we used a home-made spectroellectrochemical cell (Fig.16) equipped with a rotating silver ring as working electrode, Ag/AgCl 3 M KCl (+210mV vs. SHE) as a reference electrode and platinum as a counter electrode. The lateral surface of the working electrode, which is exposed to the electrolyte solution, is nanoscopically rough, chemically modified and used for protein immobilization. The laser light is focused onto surface of the working electrode carrying biocompatibly immobilized protein with a long working distance objective. To ensure that the same sample spot on the electrode is not exposed to long laser irradiation, in all experiments the electrode was set to rotate. The electrochemical cell of a volume of about 10 mL was extensively purged by continued flow of argon. The applied electrode potential is controlled by a potenstiostat/galvanostat (Princeton applied research Model 263A).

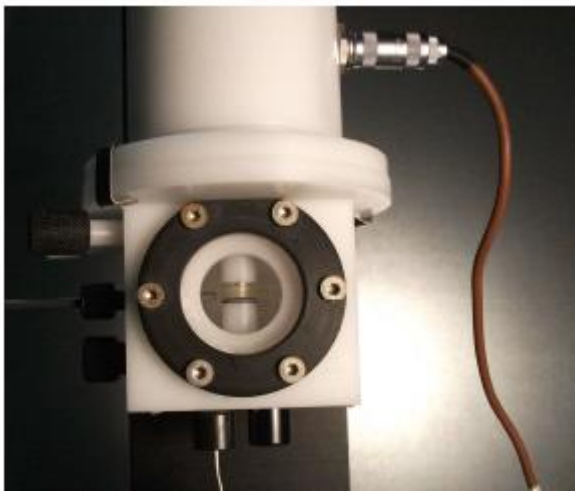

Figure 16 – *Spectro-electrochemical cell [37].*

Typically 60 μL of 128 μM protein was added to the spectroelectrochemical cell containing SERR buffer, in order to yield a concentration around 0.4 μM. At this concentration only the signal originating from the adsorbed protein can be detected, due to SER effect. Alternatively, the coated working electrode was incubated in 60 μL of 128 μM protein prior to positioning into the cell. The argon flow was maintained during the experiments, to ensure absence of oxygen in the cell. All acquired spectra were analyzed in the high-frequency region from 1300 to 1700 cm^{-1}. Each experiment wes repeated several times to ensure reproducibility of results.

- **Electrode preparation**

The role of working is twofold: i) to provide surface enhancement (i.e. SER effect) and ii) to allow control of applied potential in electrochemical studies. For that propose Ag electrodes were prepared according to the well established procedures. Ag was a metal choice since it provides SER effect in the studies employing Soret band excitement of PpDyP. Prior to protein immobilizations, the electrodes were subjected to several redox cycles. Known to result give origin to nanoscopically rough Ag surface.

Silver ring electrodes were polished with sand paper and rinsed with water then with ethanol and finally gently dried with N_2. After this the electrode is inserted into spectroellectrochemical cell and subjected to a potential of *E* = -2 V (vs. Ag/AgCl, 3M KCl) in 0.1 M KCl electrolyte solution for 20 s under stirring to reduce all possible impurities present on a surface. Subsequently, three oxidation-reduction cycles at +0.30 V and -0.30 V were applied to provide nanoscopically rough surface. Then the silver ring electrodes were rinsed with water to remove the salt and immersed for 12-24 hours in 1-2 mM ethanol solutions (purity 99.8%, Riedel-de-Haën) of ω-functionalised alkanethiol of choice to form self assembled monolayer (SAM) on the silver surface. Prior to measurement the SAM-coated electrodes were washed gently with ethanol and dried with argon and then placed into the electrochemical cell containing a SERR buffer solution (PBS 12.5 mM and K_2SO_4 12.5 mM) and protein.

- **Fit Analysis**

Contributions of each species that differ in oxidation, spin or coordination state were determined by MATLAB based software (QPipsi). A fit file was generated by fitting a set of Lorenzian bandshapes for each species, with each Lorenzian bandshape corresponding to a vibrational mode. In the analysis the spectral parameters of each species are treated as a group with fixed band position, width and relative intensity. Determination of redox potential was based on relative SERR intensities (I_i) of different heme species (the concentration of which is : $c_i = f_i\ I_i$). Due to the absence of values for the respective cross-sections, f_i, the Nernst equation was fitted directly to relative SERR intensities of each species.

4.1. Enzyme purification

4.1.1. Cloning and expression of DNA fragments

The *ppDyp* gene was cloned into the expression vector pET-21a(+) to make pRC-1, and the final construct was transformed into *E. coli* BL21*, in which expression of *ppDyp* gene could be driven upon IPTG induction of the *T7lac* promoter.

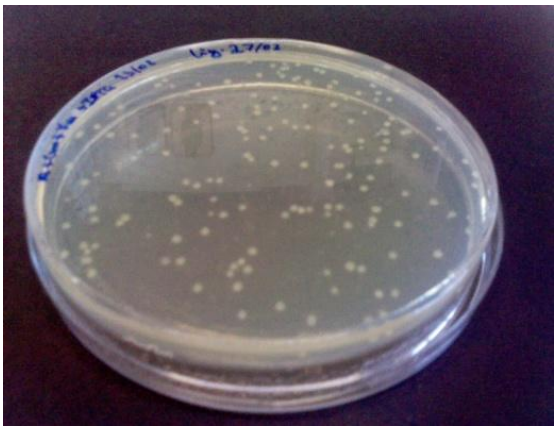

Figure 17 – *Culture plate - Colonies of the recombinant E.coli in LB medium supplemented with ampicillin.*

First, a single colony was picked from the plate and used for pre inoculum, which was grown overnight. On the next day, the pre inoculum with an initial OD_{600} of 0,05 was transferred into 1L of LB media supplemented with ampicillin and hemin and grown at 37°C. After 24h the growth was stopped avoiding the decline phase. The cells were disrupted by French press.

4.1.2. Purification by liquid chromatography

The recombinant protein was purified using two chromatographic steps.

- **Anionic exchange chromatography**

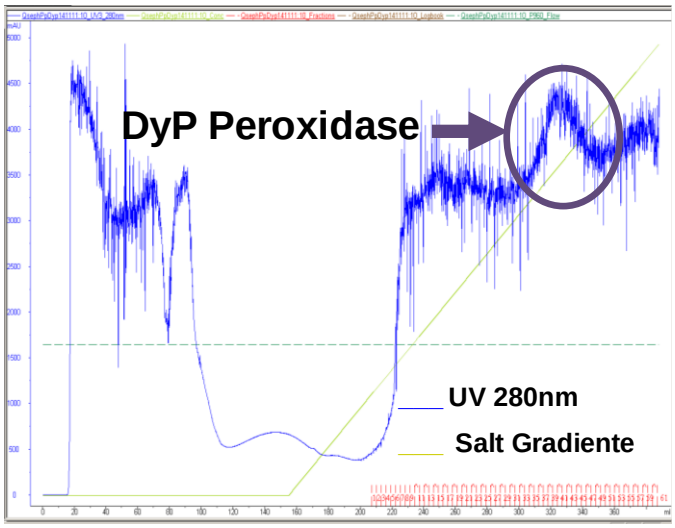

Figure 18 – *Elution profile of ion exchange chromatography using the Q Sepharose column.*

After cell disruption and centrifugation, collected supernatant was further purified. The first column was loaded with volume of approximately 5mL. Proteins began to be eluted at 45% gradient of salt. Enzyme activity assays were measured in all collected fractions to identify those which contained the PpDyP. In the activity assay, ABTS oxidation was followed: when ABTS reacts with H_2O_2 and PpDyP, a colored cation radical (oxidation form) is generated. More concentrated protein originated plates with more intense color. The colored fractions (Fig. 19) were collected and subjected to the next purification step.

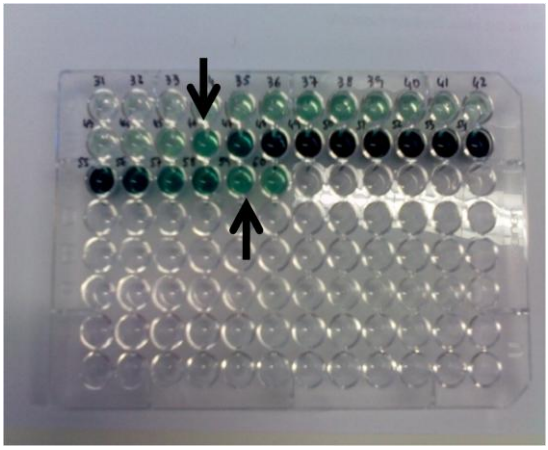

Figure 19 – Enzyme activity of ion exchange chromatography fractions. Followed via ABTS oxidation: colored fractions indicate presence of PpDyP.

- ## Size exclusion chromatography

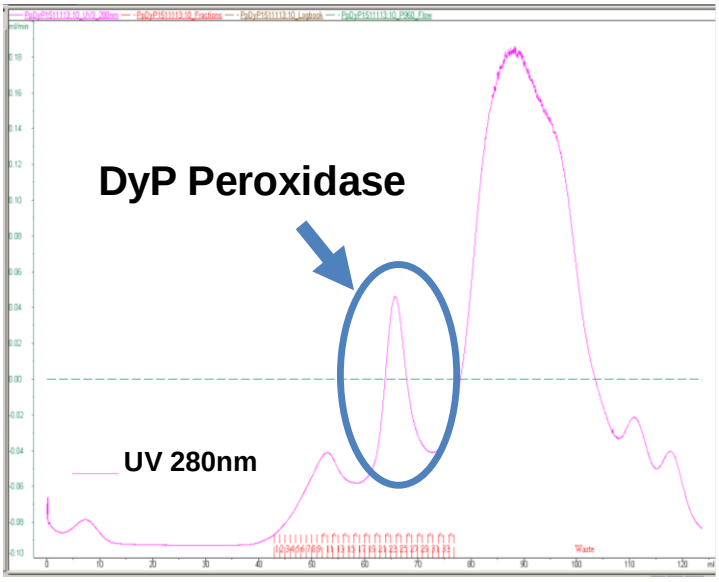

Figure 20 – *Elution profile of size exclusion chromatography using the Superdex 200.*

A fraction containing PpDyP (Fig. 21 well 2), of a volume of approximately 4 mL was loaded onto size exclusion column. Proteins began to be eluted at 50 mL of elution (Fig. 20). As described before, enzymatic activity assays (following ABTS oxidation) were employed to identify all fractions containing PpDyP. They were collected and concentrated to a final volume of 20 mL.

- **Purity analysis by polyacrylamide gel electrophoresis**

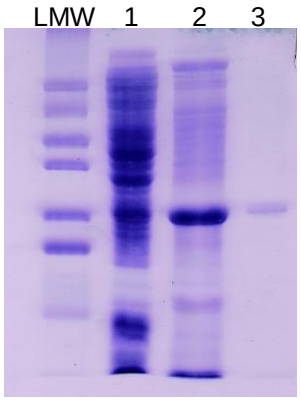

Figure 21 – *SDS-PAGE. Well 1: crude extract, well 2: sample after ion exchange chromatography, well 3: sample resulting from size exclusion chromatography and LMW: low molecular weight marker.*

Purity of PpDyP was verified by SDS-PAGE analysis based on Low Molecular Weight markers (LMW). We can conclude that PpDyP shows a high purity and an apparent molecular mass of 31.3 kDa (Fig. 21).

- **Protein quantification**

Table 2 – *Protein quantification for all purification steps.*

		Volume ***mL***	Protein ***mg***	Total Activity ***µmol/min.mL***	Specific Activity ***µmol/min.mg***	Yield %	Purification factor
(1)	**Crude extract**	5	256	440.6	1.7	100	1
(2)	**Q sepharose**	4	36	179.7	4.9	40.8	2.9
(3)	**Superdex 200**	20	14	141.7	10.2	32.2	5.8

As the table shows, the total activity measured is decreasing along the purification steps, while the specific activity of the PpDyP is increasing confirming that all protein fractions other than PpDyP are being removed from the sample. At the end of the purification 14 mg of enzyme with 10.2 μmol/min.mg of specific activity were obtained from 1L of starting medium. The yield of purification was about 32 %.

4.2. Biochemical Characterization

4.2.1. Molecular mass determination by molecular exclusion chromatography

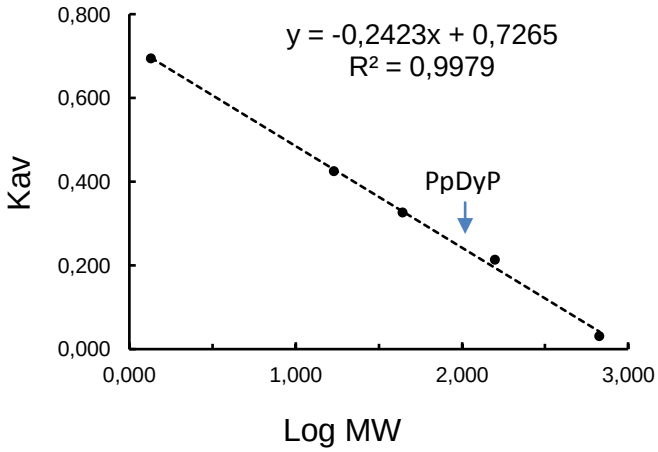

Figure 22 – *Calibration curve for determination of apparent molecular weight, where Kav is the gel-phase distribution coefficient.*

Due to denaturing conditions of MW determination, SDS-PAGE revealed that the protein was constituted by a single monomer. For a determination of real conformation of the protein, it is necessary to use the size exclusion chromatography to construct a calibration curve from the MW of standards and then extrapolate for the protein under study. Size exclusion chromatography yielded for the native PpDyP a molecular mass of 120.14 kDa, demonstrating that the recombinant enzyme forms a homotetramer in solution.

4.2.2. Protein stability

- **pH induced denaturation**

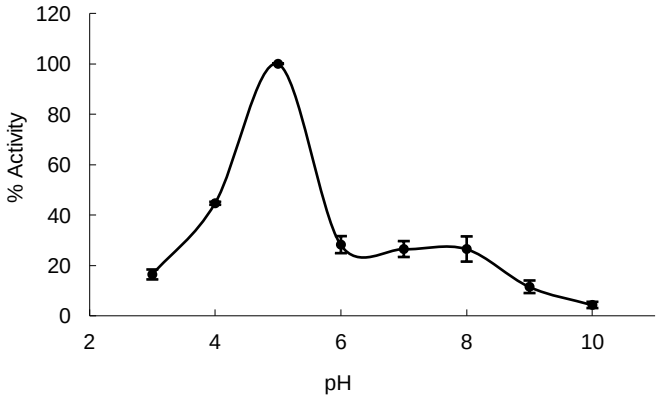

Figure 23 – *pH profile of PpDyP using ABTS as a substrate.*

By analysis of PpDyP activity as a function of pH, using ABTS as substrate we can conclude that the optimal activity pH range of PpDyP is between 4 and 6.

- **Reversible thermal denaturation**

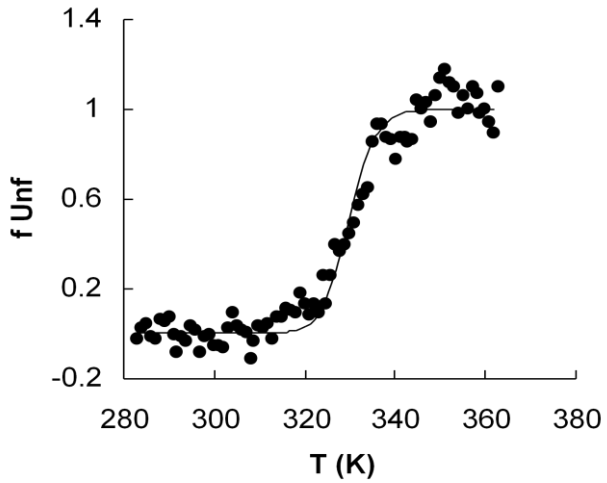

Figure 24 – *Thermal stability profile of PpDyP, where the fraction of unfolded (f Unf) protein is represented as a function of temperature.*

By analysis of the fraction of unfolded protein as a function of temperature we observe that PpDyp presents a broad range of optimal temperatures, ranging from 320 to 345K. Melting temperature is $Tm_{½}$ = 331 K (58 ºC). At this temperature there is the same amount of protein in native and denaturated state, allowing us to determine ΔS = 68 Kcal/mol (Eq. 3). This value is positive due to the denaturation process, since during the process there is an increase of microstates and this increases the disorder of the system and therefore an increase in entropy of the system [23].

- **Denaturation induced by chemical agents**

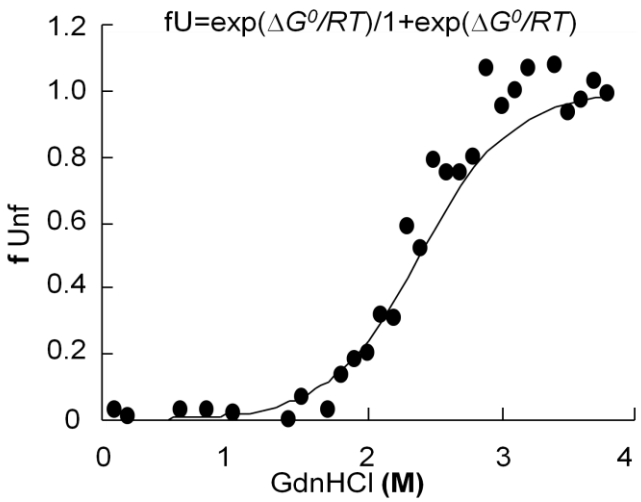

Figure 25 – *Chemical stability profile of PpDyP at pH 7,6, where the fraction of unfolded (f Unf) protein is represented as a function of concentration of chemical denaturing agent.*

Analysis of the dependence of PpDyP on concentration of GndHCl reveals a ΔG^0 = 4.12 Kcal/mol and $[GndHCl]_{½}$ = 2.4 M (Eq. 6). Therefore 2.4 M of GndHCl are required in order to obtain 50% of PpDyP molecules in unfolded state at pH 7,6.

4.3. Spectroscopy

4.3.1. UV-Visible Spectroscopy

The solution of purified enzyme was orange, indicating a presence of the heme chromophore. The UV-Visible spectrum of resting state of enzyme showed the Soret band at 406nm and the charge transfer (CT) bands at 506 and 636 nm (Fig. 26). The pyridine ferrohemochrome spectrum of PpDyp had absorption peaks corresponding to the Soret band (419nm), and to the β and α bands (527 and 556nm, respectively) that are characteristic of iron protoporphyrin. The heme content was estimated using the difference between the published [29,31] molar absorption coefficient at 556nm of the reduced and oxidized protein (ε_{556red}-ε_{556ox}) being 1.16 mol of heme b per mole of protein (heme:protein ratio of approximately 1:1). This result indicates that the protein is fully loaded with heme cofactor.

The reduction of PpDyP with sodium dithionite caused a decrease of the Soret band and its shift it to 432 nm, and appearance of a new peak at 556nm (Fig. 26). In the presence of equimolar amount of H_2O_2, PpDyp was oxidized to compound I, characterized by a shift in the Soret band to 410 nm, and the appearance of additional peaks at the absorbance of β and α bands with lower intensities. Protein was able to return spontaneously to the resting state (upon exposure to O_2) in both cases.

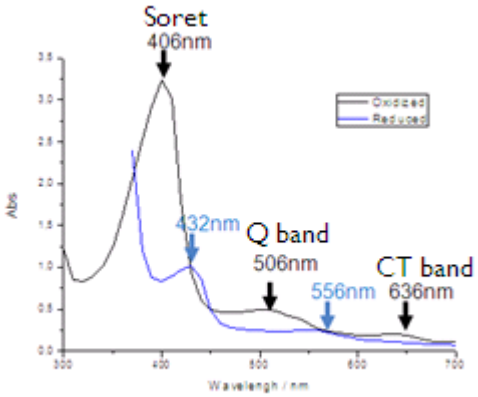

Figure 26 – *Electronic absorption spectra of 128 μM of PpDyP: as isolated (oxidized state) (black line) and dithionite reduced state (blue line).*

4.3.2. Resonance Raman spectroscopy

The resonance Raman spectra of PpDyP in solution at RT, were measured for the protein in the fully oxidized or reduced state. These spectra allowed us to determine coordination and spin states of the enzyme, and also to define spectral parameters of individual spin species, which will be later used for the analysis of the SERR spectra. The figure 27 shows the high frequency region (1200-1700 cm^{-1}) RR spectra of PpDyP in solution in fully oxidized and dithionite reduced state. The spectral range includes the marker bands ν_4, ν_3 and ν_2. Frequencies of these bands are indicative of oxidation state of iron (ν_4) and the spin, coordination and oxidation state (ν_3 and ν_2) of iron in the heme group. The RR spectra of PpDyP show that the major spin population is in both redox states, a pentacoordinated high spin (5cHS).

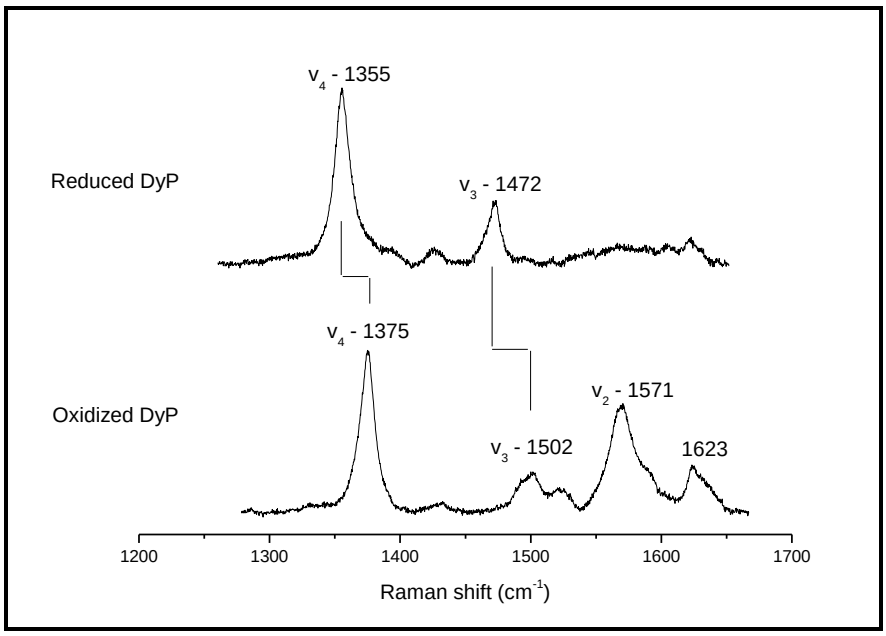

Figure 27 – *Resonance Raman spectra (1200 – 1700 cm^{-1}) of 128 μM PpDyP in the resting (bottom spectrum) and dithionite reduced (upper spectrum) states.*

Moreover, a closer look at the spectrum of the ferric protein reveals a RR fingerprint indicative of two co-existing ferric heme species that are well distinguished, in particular by the two ν_3 bands at 1492 cm^{-1} and 1502 cm^{-1} (Fig. 27).

Deconvolution of the ν_4 region employing component analysis of the spectra shows that the signal at 1375 cm^{-1} is also composed of two major Lorentzian bands at 1372 cm^{-1} (band width, $\Delta_{\nu 1372}$ = 10,2 cm^{-1}) and 1376 cm^{-1} ($\Delta_{\nu 1376}$ = 10,5cm^{-1}). In the ferrous state, a single major species, characterized by ν_3 at 1472 cm^{-1} ($\Delta_{\nu 1472}$ = 10,9 cm^{-1}) and ν_4 at 1355 cm^{-1} ($\Delta_{\nu 1355}$ = 12,9 cm^{-1}), is present in chemically reduced protein in solution. The ν_3 band at 1492 cm^{-1} together with ν_4 at 1372 cm^{-1} and ν_2 at 1570 cm^{-1} is characteristic of 5cHS population, typically found in the resting state of heme peroxidases. However, the ν_3 band at 1502 cm^{-1} is indicative of both six coordinated low spin (6cLS) and five coordinated quantum mechanically mixed-spin (5cQS) ferric heme. The electronic absorption spectrum of resting PpDyP (Fig. 26 A) bears no features of the LS heme group, allowing for putative assignment of the ν_3 1502 cm^{-1} species to a 5cQS population. This unusual heme species is characteristic for class III plant peroxidases and its unambiguous identification is commonly assessed by combination of electronic absorption and RR spectroscopies [38]. However, so far no indication for 5cQS species in DyP-type peroxidases has been reported. Interestingly, our RR and electronic absorption data show that resting PpDyP reveals pronounced similarity to HRP and other class III plant peroxidases. In the ferrous state, the frequency of ν_3 mode (1472 cm^{-1}), indicates the 5cHS species as the major spin population present in PpDyP. This finding further supports putative assignment of ferric spin population represented by ν_3 1502 cm^{-1} to QS, which unlike ferrous HS and LS species, shows no distinct RR features in the reduced form [38].

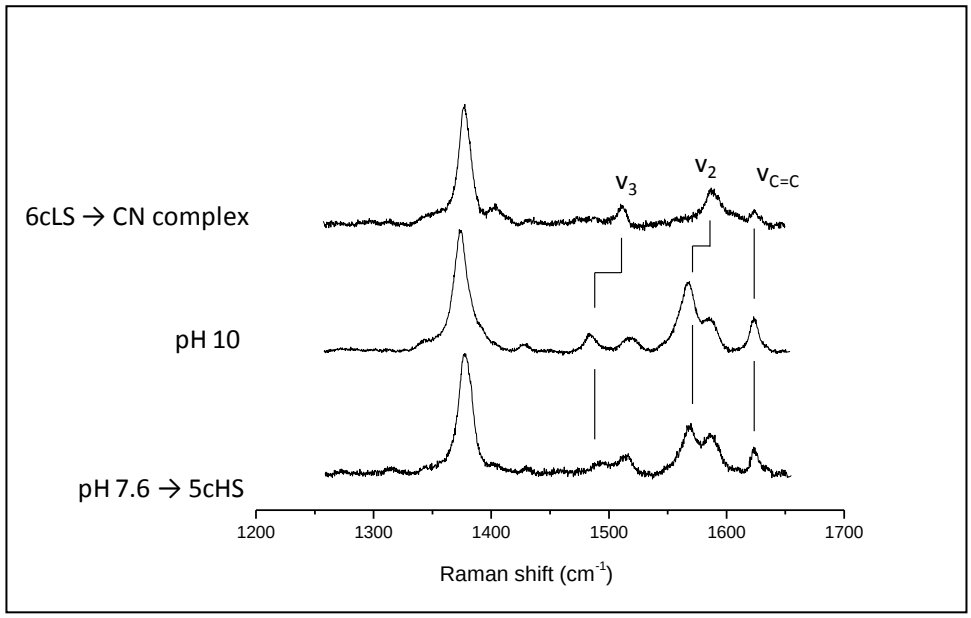

Figure 28 – *Resonance Raman spectra (1200 – 1700 cm^{-1}) of PpDyP in native state at pH 7.6, at pH 10, and with a CN complex.*

To confirm the assignment of the ν_3 1502 cm^{-} to QS, LS heme adduct were generated upon addition of excess of KCN or increase of pH. The former adduct resulted in pure 6cLS ferric complex of PpDyP (Fig. 28) with RR fingerprint distinct from that of the QS species, confirming our assignment. The Fe-OH adduct was not 6cLS indicating that the OH is not sufficiently strong ligand to induce a low spin state in PpDyP [38].

4.3.3. Immobilization of PpDyP on biocompatible Ag electrodes

Due to the absence of the x-ray structure of PpDyP and therefore knowledge of surface charge distribution of this protein, the immobilization followed trial and error strategy. Several, SAMs were tested (Table 3) in pure and mixed form, different buffer solutions (pH values and ionic strength) and various poised potentials were tried in order to provide the best conditions for protein immobilization.

Table 3 – *Trials for PpDyP immobilization at different conditions (pH, buffer and SAM composition).*

SAM	Buffer	Nº electrodes	Poised Potential	Adsorption
C_{11} (COOH)	SERR	2	-120, -70, +100	No
C_{10} (CH_3)	SERR	2	-500, -200, +100	No
C_2 (OH)	SERR	1	o c, -500, -100, +120	Yes – low
C_2 (NH_2)	SERR	1	o c, -100	No
Mixed C_2 (OH/CH_3) 1:1	SERR	2	o c, -500, -100, +100	Yes – very low intensity
Mixed C_6 (OH/CH_3) 3:1	SERR	2	o c , -400, -250 +150	Yes – low intensity
Mixed C_{11} (OH/CH_3) 3:1	SERR	2	o c , -400, +150	Yes – low intensity
Mixed C_{11} (OH/CH_3) 1:1	Britton Robinson 50 mM pH 9	2	o c , -400, -100, +120	Yes – low intensity
C_6 (NH_2)	Tris acetate 100 mM pH 8 bubbling with argon	1	o c , -500, +50, 0, -50 +100, -500 , +100	Yes – very high
Bare	Tris acetate 100 mM pH 8 bubbling with argon	2	o c , -500, +100	Yes – very high
Mixed C_6 (OH/NH_2) 3:1	Tris HCl 20 mM pH 8 bubbling with argon	3	o c , -500, -400	Yes - promising

In majority of the cases either no adsorption, or very low intensity SERR signals were obtained. After numerous trials the best conditions were identified. PpDyP was successfully immobilized on nano-structured Ag electrodes coated with mixed aminooctanethiol (AOT) and mercaptohexanol (MOH) SAMs in 1:3 (M/M) ratio (Fig. 29). Strong SERR signals of PpDyP are observed upon spontaneous adsorption (within 5 min) of the enzyme onto electrodes kept at open circuit (no applied poised potential).

Other tested coatings, including pure and mixed methyl-, carboxyl-, and pure hydroxyl- or amino-terminated SAMs, do not provide a suitable platform for immobilization, as conclude from absence of, or very weak SERR spectra. According to the values for the pK_a of amino-terminated SAMs, a considerable amount of the AOT in the mixed monolayer is protonated at pH 7, giving rise to a positive charge density on the SAM surface. Since the hydroxyl-terminated MOH is also essential, we conclude that the enzyme requires a surface with "diluted" positive charge for adsorption [38].

4.3.4. Surface Enhanced Resonance Raman

The immobilized PpDyP retains its structural integrity on the level of the heme group upon adsorption, as revealed by comparison of SERR with RR spectra (Fig. 29).

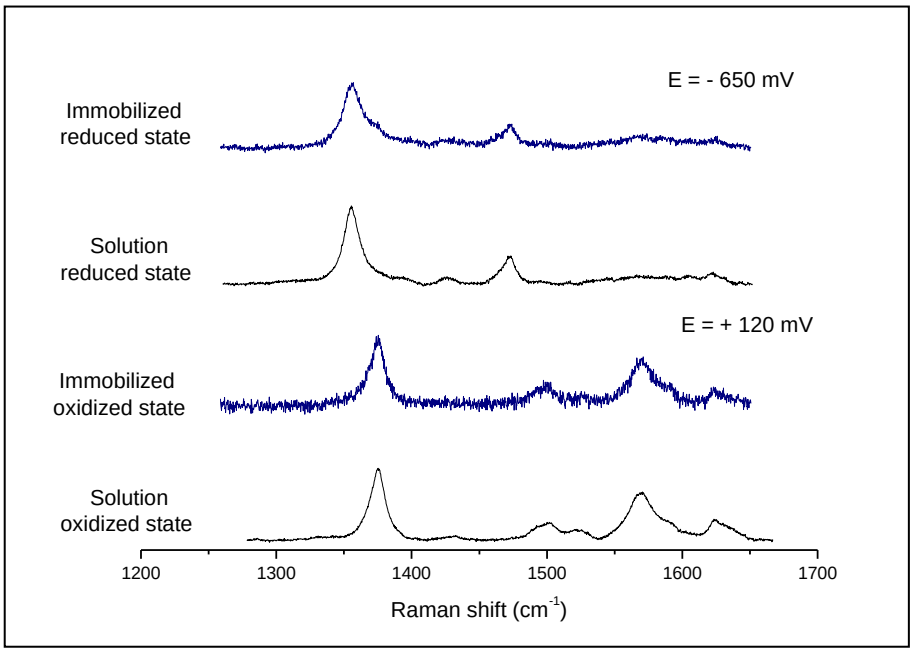

Figure 29 – *RR spectra of PpDyP in solution, in oxidized and reduced states and SERR spectra of immobilized PpDyP on a mixed C8 amino – C6 mercapto-1-hexanol (1:3) recorded at +0.120V (oxidized) and -0.650V (reduced) (vs. Ag/AgCl).*

Moreover, the immobilized enzyme sensitively responded to changes of the electrode potential in a reversible manner, as judged by the oxidation state marker bands in the high frequency region of the SERR spectra. Hence, PpDyP is electronically coupled to the electrode. At positive electrode potentials, SERR spectra of the immobilized enzyme display no major differences with respect to the RR spectra of resting PpDyP in solution. Similarly, electrochemically reduced adsorbed protein and chemically reduced PpDyP in solution reveal almost identical spectra.

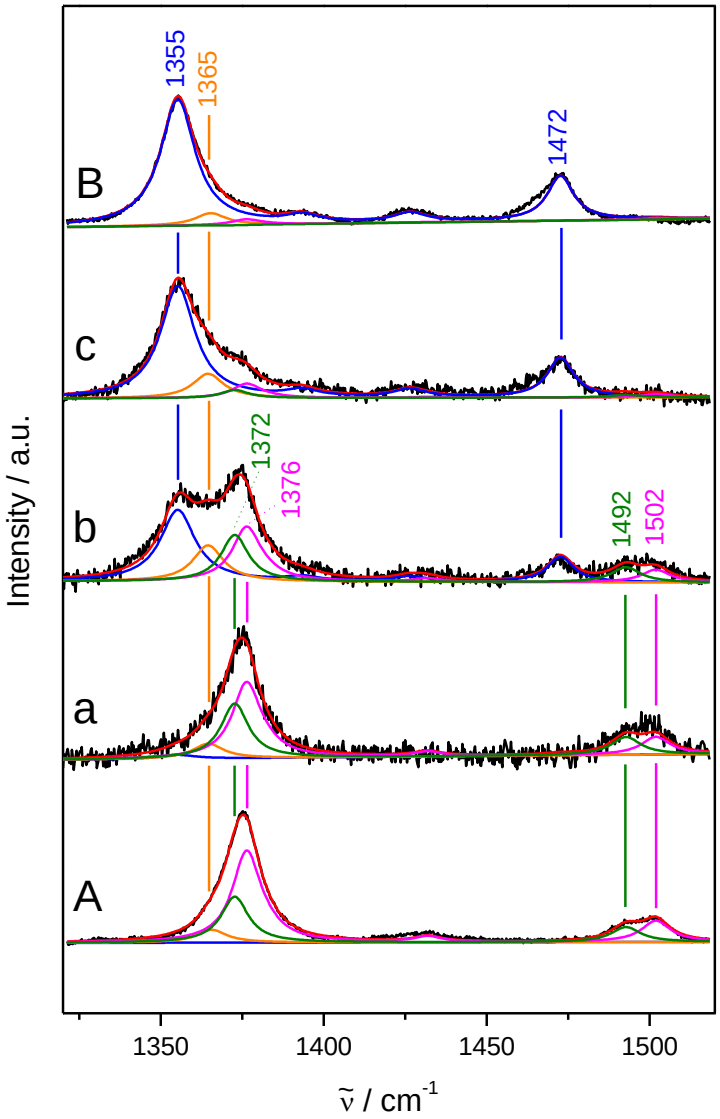

Figure 30 – *Component analysis of RR spectra (1300 – 1550 cm^{-1}) of ferric (A) and ferrous (B) PpDyP in solution; and SERR spectra at +0.23 V (a), -0.29 V (b), and -0.44 V (c) electrode potential. The black and red lines are the baseline corrected experimental spectra and the sum of contributions from different species (resulted from component analysis), respectively. Magenta represents the ferric 5cHS, green the ferric 5cQS, blue the ferrous 5cHS species. The contribution of the electro-inactive species is represented in orange.*

The SERR measurements were also carried out for PpDyP directly adsorbed onto the surface of the silver electrode in the absence of SAM (bare electrode). The spectrum differ significantly from RR spectra, indicating that denaturation of the protein occurred.

Table 4 – *(SE)RR spectral parameters of after fitting of PpDyP of different heme species.*

	ν_4 (cm^{-1})	ν_3 (cm^{-1})
5cHS (Fe^{3+})	1372	1492
5cQS	1376	1502
5cHS (Fe^{2+})	1355	1472
Non native	1364	-

Component analysis of SERR spectra recorded at different potential applied to the coated (C_8-NH_2:C_6-OH) working electrode revealed a small amount of non-native protein (ν_4 at 1364 cm^{-1}) (Fig. 30), which is not sensitive to the change of electrode potential. Contribution of this species was subtracted from the ν_4 contributions of redox-active species in the further analysis.

4.3.5. SERR spectroelectrochemistry

Redox properties of the immobilized PpDyP were studied by SERR spectro-electrochemistry by recording SERR spectra at different potentials imposed to the working electrode. The contributions of the ferric and ferrous species at each poised potential were determined from component analysis of potential dependent SERR spectra in the 1300 cm^{-1} to 1520 cm^{-1} range. This interval includes the ν_3 and ν_4 modes, which are sensitive indicators of the heme oxidation and spin state, respectively, and, in addition, largely free of uncertainties related to spectral parameters of several overlapping bands in the ν_2/ν_{10} region of the ferric proteins. In the ferrous state poorly resolved spectral features in the ν_2/ν_{10} region further impede reliable analysis of this region. Potential dependence of relative spectral contributions of the two ferric (ν_4/ν_3: 1372 cm^{-1}/1492 cm^{-1} and 1376 cm^{-1}/1502 cm^{-1}) and one ferrous (1355 cm^{-1}/1472 cm^{-1}) species reveals a sigmoid shape (Fig. 31). In the analysis, the spectral parameters of each species are treated as a group with fixed band positions, widths and relative intensities. As revealed by the plots, the protein is predominantly (~95%) oxidized at the most positive potential and 90-95% reduced at the most negative applied potential, indicating that the three major spin populations are fully electroactive in the immobilized state and exhibit reversible heterogenous ET within the studied potential range. In the contrast, the ET-inactive species (ν_4 1364 cm^{-1}) irreversibly gains intensity with time. It accounts for about 10% of the overall ν_4 intensity in the beginning of SERR experiments. After ca. one hour under typical experimental conditions (exposure to several electrode potentials and laser irradiation) this percentage is doubled. Due to accelerated accumulation of the ET-inactive species upon prolonged and/or intense laser irradiation, laser power and accumulation times were kept to a minimum to reach a compromise between the spectral quality and stability of the adsorbed enzyme [38].

The fit of the Nernst equation to the relative spectral contributions of two ferric species as a function of electrode potential reveals similar E_m values around -0.3V, and low values for n_{app} ($\leq$ 0.5). As expected, the redox transition of the ferrous species coincides with this E_m value. The midpoint potential of PpDyP in solution, $E_{m,sol}$, obtained by potentiometric titration followed by electronic absorption spectroscopy, is equal to -0,26V, with $n_{app,sol}$ equal to one [38].

The sharp redox transition of two ferric to the same ferrous species take place without deviation from the ideal Nernst behavior, providing additional evidence for close midpoint potential of the ferric species. It must be noted, however, that the redox transition of immobilized PpDyP is broad, yielding $n_{app} < 1$. This can be rationalized in terms of a broad distribution of midpoint potentials originating from different orientations of individual enzyme molecules with respect to the electrode surface.

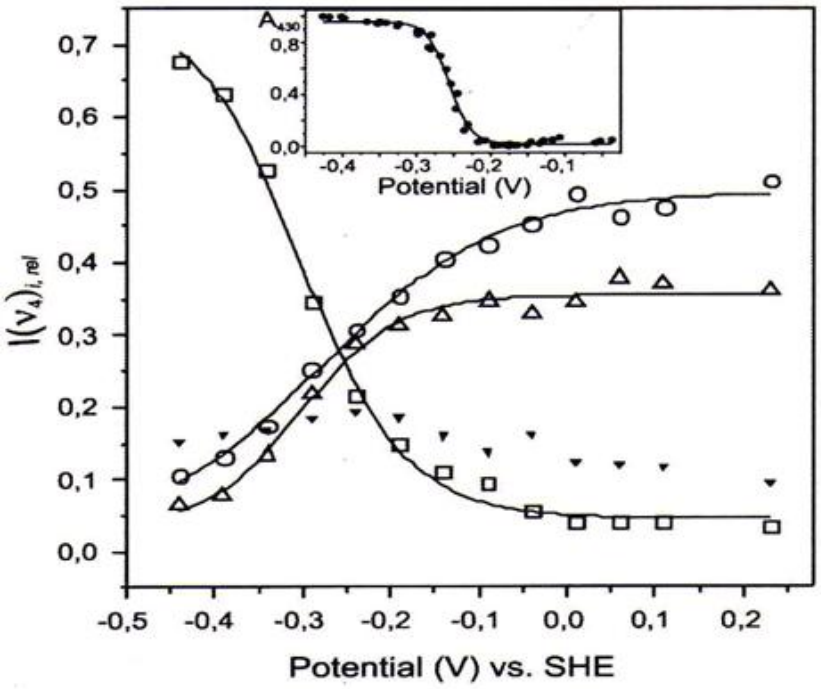

Figure 31 – *Potential dependent relative SERR contributions ($I(\nu_4)_{i,rel}$) of heme species as obtained from component analysis. Hollow squares: ferrous 5cHS, hollow circles: ferric 5cQS, hollow triangles: 5cHS species, solid triangles: ET-inactive species. The solid lines are fits of sigmoid functions to data [38].*

5. CONCLUSIONS/ FUTURE PERSPECTIVES

The development and use of biosensors has been an important breakthrough in several areas. New techniques and materials are tested and this increased the possibilities for applications. The use of biosensors for early detection and treatment of disease became an important tool in general medicine and for the development of new drugs. Highlights also include the use of biosensors in the detection of chemical substances in environments such as soils, water and food. As the detection of these agents is generally delayed, the risk of contamination becomes larger. In this case, biosensors allow a real-time analysis and *"in locus"*, which favors a rapid action against pollution.

In the development of biosensors the enzyme must be purified and then immobilized by physical or chemical methods. The choice of best method for immobilization is directly related to preservation of the active site structure of the enzyme, its catalytic activity and the performance of the biosensor. Higher enzyme activity and stability after immobilization provides the best sensitivity of the biosensor.

This work is based on PpDyP, a new member of a novel class of peroxidases. It has a high potential for development of biosensors, due to its capacity to decolorize structurally diverse inert dyes. We show that it can be immobilized on biocompatible support under preservation of its structural and thermodynamic features, which is a prerequisite for development of DyP-based biosensor or biocatalyst. First, we developed a procedure for overexpression and purification of this promising enzyme in large quantities. Then, we employed a sensitive experimental tool that allowed us to characterize this novel enzyme in solution and immobilized state. Taken together, our results show that the DyP represents a good candidate for design of enzyme electrodes that can function as biosensors or biocatalysts. In the next step we aim to construct a functional device, and identify, design and produce PpDyP mutants with improved catalytic performance in bioelectronic devices.

6. REFERENCES

1. FITZGERALD-HAYES, M. ; REICHSMAN, F. - DNA and Biotechnology, 3th Edition, Elsevier, 2010
2. MURGIDA, D. ; HILDEBRANDT, P. ; TODOROVIC, S. - Immobilized redox proteins: mimicking basic features of physiological membranes and interfaces in Biomimetics learning from nature, IN-TECH Vienna, 2010
3. OGOLA, H. [et.al] - Molecular characterization of a novel peroxidase from the Cyanobacterium Anabaena sp. Strain PCC 7120, Applied and Environmental Microbiology, 2009, 75, 7509-7518
4. OGOLA, H. [et.al] - Enhancement of hydrogen peroxide stability of a novel Anabena sp. DyP-type peroxidase by site-directed mutagenesis of methionine residues, Appl Microbiol Biotechnol, 2010, 87, 1727-1736
5. SUGANO, Y. - DyP-type peroxidase comprise a novel heme peroxidase family, Cellular and Molecular Life Sciences, 2009, 66, 1387-1403
6. VEITCH, N. C. - Horseradish peroxidase: a modern view of a classic enzyme, Phytochemistry, 65, 2004, 249-259
7. PeroxiBase – The peroxibase database in https://peroxibase.toulouse.inra.fr/
8. BERGLUND [et.al] - The catalytic pathway of horseradish peroxidase at high resolution, Nature, 2002, 417, 463-468
9. DUNFORD [et.al] - Peroxidases and Catalases: Biochemistry, Biophysics, Biotechnology and Physiology, 2nd Edition, 2010, John Wiley and Sons Inc.
10. Horseradish Peroxidase in http://chemwiki.ucdavis.edu/Biological_Chemistry/Catalysts/Case_Studies/Horseradish_Peroxidase
11. TORRES, E. ; AYALA, M. - Biocatalysis Based on Heme Peroxidases, Springer, 2010
12. BERTINI, I. ; SIGEL, A. ; SIGEL, H. - Handbook on Metalloproteins, Marcel Dekker Inc., 2001
13. YOSHIDA, T. [et.al] - The catalytic mechanism of dye-decolorizing peroxidase DyP may require the swinging movement of an aspartic acid residue, The FEBS Journal, 2011, 278, 2387-23941

14. SUGANO, Y. ; ISHII, Y. ; SHODA, M. - Role of H164 in a unique dye-decolorizing heme peroxidase DyP, Elsevier, 2004, 322, 126-132

15. SHIMOKAWA, T [et.al]. - Efficient Dye Decolorization and Production of Dye Decolorizing Enzymes by the Basidiomycete Thanatephorus cucumeris Dec 1 in a Liquid and Solid Hybrid Culture, Journal of Bioscience and Bioengineering, 2008, 106, 481-487

16. SUGANO, Y. [et.al] - Matsushima Y., Tsuchiya K., Aoki H., Hirai M., Shoda M., Degradation pathway of na anthraquinone dye catallyzed by a unique peroxidase DyP from Thanatephorus cucumeris Dec 1, Biodegradation, 2009, 20, 433-440

17. MARTINHO, M. G. M. ; GONÇALVES, M. G. P. - Gestão de Resíduos, Universidade Aberta, 1999

18. ERDEM, A. [at.al] - Electrochemical Biosensor Based on Horseradish Peroxidase for the Determination of Oxidizable Drugs, Turk J Med Sd, 2000, 30, 349-354

19. GRAY, H. ; WINKLER, J. - Electron Transfer in Proteins, Annu Rev Biochem, 1996, 65, 537-561

20. SUGANO, Y. ; MATSUSHIMA, Y. ; SHODA, M. - Complete decolorization of the anthraquinone dye Reactive blue 5 by concerted action of two peroxidases from Thanatephorus cucumeris Dec 1, Appl. Microbial Biotechnol, 2006, 73, 862-871

21. PETRIDES, P.E. ; NAUSEEF, W. M. - The Peroxidase Multigene Family of Enzymes, Biochemical Basis and Clinical Applications, Springer

22. SUGANO, Y. [at.al] – A Unique Dye-decolorizing Peroxidase, Represents a Novel Heme Peroxidase Family ASP^{171} Replaces the distal histidine of classical peroxidase, Journal of Biological Chemistry, 2007, 282, 36652-36658

23. CABRAL, J. M. G. ; AIRES-BARROS, M. R. - Gama M., Engenharia Enzimática, Lidel, 2003

24. BERG, J. M. ; TYMOCZKO, J. L.; STRYER, L. - Biochemistry, 5th Edition, New York: W. H. Freeman, 2002

25. SIEBERT, F. ; HILDEBRANDT, P. - Vibrational Spectroscopy in life science, Wiley-VCH, 2008

26. BERRY, E. ; TRUMPOWER, B. - Simultaneous Determination of Hemes a, b, and c, from Pyridine Hemochrome Spectra, Analytical Biochemistry, 1987, 161, 1-15

27. ROBERTS, J. [at.al] - Characterization of Dye-Decolorizing Peroxidases from Rhodococcus jostii RHA 1, Biochemistry, 2011, 50, 5108-5119
28. CHRISTIANE, J. - The mistery of cytochrome P450 Compound I, Biochimica et Biophysic Acta, 2011, 1814, 46-57
29. SCHRADER, B. - Raman and Infrared Atlas of Organic Compounds, 2nd Edition, VCH-Verl., 1989
30. SOLOMON, E. ; LEVER, A. - Inorganic Electronic Structure and Spectroscopy, Volume I: Methodology, Wiley-VCH, 2006
31. SMITH, E. ; DENT, G. - Modern Raman Spectroscopy – A Practical Approach, John Wiley & Sons Ltd, 2005
32. HU, S. [et.al] - Complete Asignment of Cytochrome c Resonance Raman Spectra via Enzymatic Reconstitution with Isotopically Labeled Hemes, J. Am. Chem Soc., 1993, 115, 12446-12458
33. SEZER, M. - Oral Presentation, Berlin, January, 2012
34. SAMANTA, D. ; SARKAR, A. - Immobilization of bio-macromolecules on self-assembled monolayers: methods and sensor applications, Chemical Society Reviews, 2011, 40, 2567-2592
35. MINTEER, S. D. - Enzyme stabilization and Immobilization: Methods and Protocols, Humana Press, 2011
36. ULMAN, A. - Formation and Structure of Self-Assembled Monolayers, Chemical Reviews, 1996, 96, 1533-1554
37. SEZER, M. - PhD Thesis - Spectro-Electrochemical Investigations on Immobilized Heme Proteins, Technical University of Berlin, 2011
38. SEZER, M. [et.al] - A Dye-type peroxidase at a bio-compatible interface: structural and mechanistic insights, Soft Matter, 2012, in press DOI: 10.1039/c2sm26310f
39. HARVEY, D. - Modern Analytical Chemistry, MC Graw Hill, 2000

APPENDIX I - Cloning and expression of DNA fragments

Molecular cloning of DyP was performed by inserting a DNA fragment of interest in a molecule called vector, which is capable of replicating independently in a host cell. The result of this process is a recombinant molecule, composed of the inserted DNA and the vector sequences. To obtain large amounts of the DNA insert is replicated in a recombinant molecule suitable host. The following explains in detail the characteristics of the plasmids, since it is the vector used to clone DNA fragments of the DyP, obtained by PCR.

Plasmid - pRC1: plasmid contains an origin of replication (ORI), an antibiotic resistance gene for ampicillin (Amp^r) and multiple restriction sites (EcoRI, BamHI, HindIII,...) (Fig. 32).

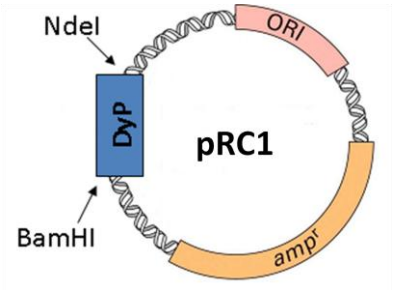

Figure 32 – *Schematic restriction map of pRC-1.*

To clone a DNA fragment into a vector, we treated the vector and the DNA with the same restriction enzymes to generate cohesive ends, then joined these fragments with DNA ligase and their union is produced by inserting the DNA into the vector. To verify that the cloning was successful, the vector was introduced into suitable host cells (*E.coli*) by thermal shock. As the vector has an antibiotic resistance gene, cells are grown in plates with medium containing the same antibiotic, (so that the cells that grow in this environment have the vector with the insert DNA) to remove all cells that do not passes properly inserted plasmid.

APPENDIX II - Purity analysis by polyacrylamide gel electrophoresis

Along the protein purification, it is necessary to estimate the effectiveness of the process. The purity of biological samples can be determined by polyacrylamide gel electrophoresis under denaturing conditions (SDS-PAGE). Peroxidase monomer has a molecular mass between 30 and 50 kDa, indicating that intermediate pore gels (10-12%) should be employed for separating proteins between 10 and 90 kDa. Working under denaturing conditions, proteins are negatively charged. The amount of SDS bound to the protein is directly proportional to its size, therefore, proteins are separated according to their molecular mass. Employing electrophoresis we can estimate the molecular weight (MW) of the protein in monomeric form with an error of ~ 10%. The higher electrophoretic mobility corresponds to the lower molecular size. With a kit of known molecular mass proteins and measured the distance of migration in the gel, can construct a calibration curve, representing the relative mobility (Rf = distance traveled by the protein band (mm)/distance traveled by bromophenol blue dye (mm)) of each protein versus log (M). Thus, by measuring the relative mobility of the protein and interpolating, can determine its molecular mass. SDS-PAGE technique has a high resolving power, because it uses a discontinuous electrophoretic system consisting of two gels of different porosity and pH. The superior, called concentrator, compact the samples and the lower, called separator, separates them. A final protein concentration ~ 0.5 mg ml^{-1} was used.

APPENDIX III - Solutions

LB medium:

- Tryptone 10 g / L
- Yeast extract 5 g / L
- Sodium chloride 10 g / L

Separation Gel (10%):

The acrylamide was mixed with upper Tris-HCl, Temed (Sigma), distilled water, SDS 10% (Sigma) and APS 10% (Sigma). After gentle agitation, the mixture was spread on 15 x 16 cm glass plates.

Gel concentration (4%):

After polymerization of separation gel, the gel was prepared in concentration, containing acrylamide, lower Tris-HCl, SDS 10% (Sigma), Temed (Sigma) and APS 10% (Sigma). This mixture was placed on the gel separation, into which a comb was inserted in order to allow formation of channels until the polymerization of the gel.

Loading buffer under reducing conditions:

20 mM TRIS pH 8.0, 10% glycerol (v:v), 2 mM EDTA, 0.001% bromophenol blue (m:v), 0.2% SDS (m:v) and 4% β - mercaptoethanol (v:v).

Electrophoresis buffer:

25 mM Tris-HCl , pH 8.3, 250 mM glycine and 0.1% SDS (m:v).

Staining solution:

Place about 30 mL of this solution, this quantity should be sufficient to submerge all gel and leave under constant agitation until protein bands appear (1 h). Constitution of the gel: 10% glacial acetic acid (v:v), 45% ethanol (v:v), 45% water (v:v) and 0,25% Coomassie blue (m:v).

Distaining solution:

Leave the gel in distilled water over night or leave 40 min in a solution of glacial acetic acid:ethanol:water (1:3:6 v:v:v).

APPENDIX IV - Molecular mass determination by molecular exclusion chromatography

This type of chromatography is widely used in biochemical purification, separating substances according to their molecular mass. Therefore, using this method, proteins are easily separable from ions or smaller molecules [39]. To perform this technique it is necessary use columns containing different types of stationary phase: cross-linked dextran (Sephadex), agarose (Sepharose) or polyacrylamide (Bio-gel B). All these matrices are composed of a spongy hydrated material that contains pores with certain size. In function of the molecules were used to separate one or the other [39]. In this case, we determine the molecular mass of the protein in native state and therefore the technique is also used to determine the degree of protein aggregation. The particles are separated in order of increasing size. Bigger proteins cannot penetrate into the pores of the gel, will move through the dead volume of the column and leave early. In contrast, smaller, can penetrate into the pores and will come out later. Small molecules will be retained in the pores of the gel and the elution volume or time will be much higher. We can relate the elution volume with molecular mass using a calibration kit containing proteins with known molecular masses, for that we passed in duplicate, each protein of the kit through the column, measuring the corresponding volume of elution, then with these data can construct a calibration curve. Finally, pass under the same conditions the protein of interest, and interpolating can obtain the molecular mass.

FIGURES LIST

TABLES LIST